Spectroscopy of the transition state. II. F+Na2→FNaNa‡→NaF+Na

P. Arrowsmith, S. H. P. Bly@f@f, P. E. Charters, and J. C. Polanyi

Citation: J. Chem. Phys. **79**, 283 (1983); doi: 10.1063/1.445522
View online: http://dx.doi.org/10.1063/1.445522
View Table of Contents: http://jcp.aip.org/resource/1/JCPSA6/v79/i1
Published by the AIP Publishing LLC.

Spectroscopy of the transition state. II. $F+Na_2 \rightarrow FNaNa^{\ddagger *} \rightarrow NaF+Na^*$

P. Arrowsmith, S. H. P. Bly,[a] P. E. Charters, and J. C. Polanyi

Department of Chemistry, University of Toronto, Toronto, Canada M5S 1A1
(Received 31 January 1983; accepted 3 March 1983).

Chemiluminescence from the reaction $F + Na_2 \rightarrow NaF + Na^*$ ($3\,^2P$) has been studied in crossed uncollimated beams at a reagent pressure of $\sim 10^{-5}$ Torr, with systematic variation of experimental conditions. The atomic *D* line emission is accompanied by "wing" emission extending over several hundred angstroms, to either side of the *D* line. The source of the wing emission has been examined in some detail. The earlier proposal [J. Chem. Phys. **73**, 5895 (1980)] that the wing comprises the emission spectrum of transition states $FNaNa^{\ddagger *}$ which exist as the reaction products are in the process of separating, is in best accord with the observations. The kinetics, spectral shape, and intensity of the wings provide the principal clues as to their origin. The red and blue wings differ in shape. The integrated intensity in the red is approximately twice that in the blue. Alternative models are considered.

I. INTRODUCTION

Progress has been made over the past two decades in characterizing reactive configurations intermediate between reagents and products. The field of reaction dynamics, which yields this information, depends on studies in which the motions of newly born reaction products, preferably formed from state-selected reagents, are used as clues to the forces operative during the reactive encounter. Since the product motions represent the integral of a varied sequence of events, as old bonds dissolve and new ones form, it is not possible to perform a unique inversion from the product motions to the reaction dynamics. Instead one must be satisfied with a type of analysis in which, first of all, theory is used to identify differing categories of dynamics, and then the product attributes are used in order to select among these categories. The greater the range and variety of measurable attributes, the less ambiguous are the inferences regarding the reaction dynamics.

The studies described in the previous paragraph come under the heading of the (optical or, in molecular beams, translational) spectroscopy of reactants and products. It is natural to ask whether such studies could in favorable cases be complemented by a spectroscopy of states intermediate between reagents and products—i.e., by a "spectroscopy of the transition state."[1] If the spectroscopy is optical then one would be probing the reacting particles at successive intermediate configurations on the reactive potential-energy surface (pes) of interest, by recording the rate at which the reacting species are transferred to some optically linked higher pes (by light absorption) or lower pes (by light emission). The subsequent analysis will be simplified by the fact that the measured quantity relates more directly to localized regions on the reactive pes, and will be complicated by the fact that a knowledge of some optically linked pes is also required. It is possible to envisage cases in which the simplification more than offsets the complication; e.g., the optically linked pes may be calculable, as in the case of H_3,[2] or may have been characterized, or may be constant in energy ... as will be suggested for some regions of configurations in the example under study here; Sec. IV. In either case a novel approach to the conundrum of reaction dynamics can be expected to yield a novel set of clues, which supplement the existing ones in an informative way. Model calculations lend credence to this view.[1-3]

The availability of intense lasers has prompted extensive theoretical discussion of the possibility of detecting the interaction of laser radiation with transitory species $ABC^{\ddagger}$, intermediate between reagents A + BC and products AB + C.[4] This would be the reactive analog of radiation assisted energy transfer which has now been observed experimentally for electronic energy transfer, charge transfer, Penning ionization, and associative ionization.[5] Preliminary evidence for transition state absorption at $\lambda = 6060$ Å was reported in a crossed molecular beam study of the reaction $K + HgBr_2 - KBr^* + HgBr$,[6] but later work (designed to move from single-wavelength absorption to a spectroscopic study) has so far failed to confirm this.[7] Meanwhile evidence has been obtained of transition state absorption at $\lambda = 1580$ Å (XeF* laser) under bulb conditions, in the reaction $Xe + Cl_2 - XeCl^* + Cl$[8]; thus lending credence to an earlier proposal by Dobov *et al.*[4(c)] The wavelength of an ArF laser (1933 Å) is thought to be too long to supply the endoergicity of this reaction; no XeCl* fluorescence was observed with this source in the work of Ref. 8. However, a concurrent study of the same system in another laboratory yielded XeCl* from ArF (1933 Å) irradiation, indicative of a two-step process; $Xe + Cl_2 + h\nu - (XeCl_2)^*$ followed by $(XeCl_2)^* + M - XeCl^* + Cl$.[9] Further work is required to reconcile these findings.

Spectroscopy of a transition state in emission has been reported in an earlier communication from this laboratory.[10] The present paper extends and details the findings, which are for the reaction

$$F + Na_2 - FNaNa^{\ddagger *} - NaF + Na^*(3\,^2P) \qquad (1)$$

[a] Princess Margaret Hospital, Department of Medical Biophysics, University of Toronto, Toronto, Ontario, Canada M5S 1A1.

 0021-9606/83/130283-19$02.10

studied at the intersection of crossed uncollimated sprays of reagent, at reagent pressures of $\sim 10^{-5}$ Torr. Emission ascribed to $FNaNa^{\ddagger}*$ was recorded over an interval of several hundred angstroms to either side of the D line. The intensity of this "wing" emission was in accord with that anticipated for labile $FNaNa^{\ddagger}*$ separating to give products.[10,11] In addition the emission profile (centered on the D line) and the kinetics indicated that the wings arose from the transition state $FNaNa^{\ddagger}*$. All these questions are subjected to closer scrutiny in the present work.

Emission from transition states $FNaNa^{\ddagger}*$, or $ABC^{\ddagger}*$ in general, can be regarded as a special case of pressure broadening. In the special case of reactive broadening the emitter $C*$ invariably encounters the partner responsible for the broadening AB, since $C*$ can only be formed by way of $ABC^{\ddagger}*$.[11] The reactive case is also distinguished by the fact that the "pressure" broadened wings must be unaltered in intensity relative to the line center, even at vanishingly low pressure. The intensity of the wings relative to the atomic line depends only on the time that $ABC^{\ddagger}*$ spends *en route* to AB + C*; this in turn depends on the reaction dynamics, but not on the reagent pressure.

The study of far wing emission in nonreactive encounters, such as rare gas (RG) plus $Na*(3\,^2P)$ collisions (here the pressure of collision partner does determine the ratio of the wing intensity to that of the atomic line), has yielded valuable information regarding the interaction potential.[12] Theoretical interpretation customarily involves assuming a constant radiative transition probability to the ground state as the Na*–RG separation varies, and then interpreting the wavelength of the observed emission in terms of the quasistatic theory[13] (QST; equivalent to the classical Franck–Condon principle) according to which emission at frequency ν is due to vertical transitions from an upper pes V_u to a lower pes V_l, such that $h\nu = V_u - V_l$. The emission intensity at a particular frequency ν is proportional to the probability of the system being found in configurations such that $h\nu = V_u - V_l$. This approximation has been used with considerable success in recent years, particularly by Gallagher and co-workers to obtain $V_u(R)$ and $V_l(R)$ where R is the internuclear separation M*–RG and M* is an excited alkali metal atom.

For the case of chemiluminescence during a *reactive* encounter, an ensemble of trajectories on the upper surface gives the probability of finding the system at configurations corresponding to emission at some frequency ν. We have previously presented a model for generating reactive wing spectra based on the QST and a constant transition moment throughout the collision.[3] This simple model presents a framework within which the experimental results presented here may be discussed.

Though reaction (1) is not itself a well-studied process, analogs to reaction (1) have been extensively studied since the early diffusion flame work.[14] Magee[15] suggested, using qualitative symmetry arguments, that reaction (1) and its analogs should be rapid, and comparable in rate to the corresponding reaction to form ground state atoms. Recently,[16,17] molecular beam studies showed conclusively that the reaction $Cl + Na_2 \rightarrow NaCl + Na*(3\,^2P)$ had a cross section of 10–100 Å^2 and was the source of D line emission under single collision conditions. Valuable dynamical information on the reaction of $X + K_2 \rightarrow KX + K*(4\,^2P)$ with X = Cl, Br was also obtained in the beam studies from the product KX angular distributions,[17] which surprisingly showed backward peaking.

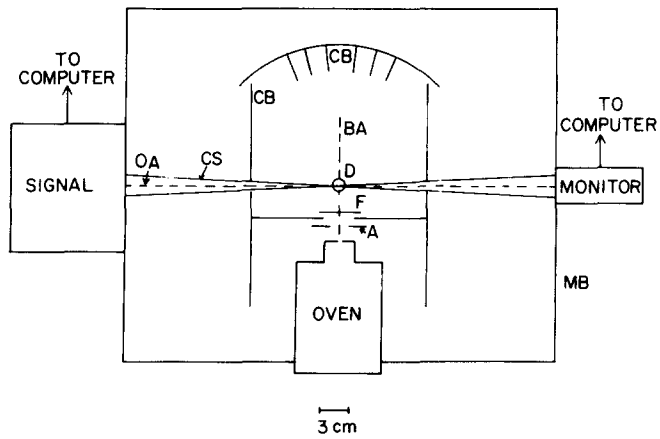

FIG. 1. Reaction vessel and associated experimental apparatus viewed from above. MB—Monel box; CB—copper baffles: F—sodium beam flag; D—discharge tube; BA—sodium beam axis; CS—spectrometer cone of sight: A—heated aperture.

The $X + M_2$ reactions (where X is a halogen and M_2 is an alkali dimer) have also been studied theoretically using a number of approximations.[18–21] The general conclusions from these studies were that the XMM systems exhibited a potential well in both the ground and excited states, and that the deepest well was in the isosceles configuration. In addition, the $X + M_2$ systems were characterized by long range interactions in the exit channels of the reactions.[19–21]

The transition state emission is discussed here in terms of the long range interactions in the exit channel of reaction (1), and the analogous reaction to form ground state Na.

II. EXPERIMENTAL

The reaction vessel, shown in Fig. 1, has been described previously.[22,23] In the present experiments, the Welsh cell and LN_2 reservoir were removed. Water cooled copper baffles replaced the LN_2 cooled reservoir. The baffles (Fig. 1) allowed the optical axis to pass at 90° through the sodium beam axis while ensuring that no sodium covered surfaces fell within the cone of sight of the spectrometer. This precaution was taken since halogens reacting at a fresh sodium surface have been shown to yield continuum emission.[24] The baffles also prevented sodium from depositing on the windows of the reaction vessel. In the majority of experiments the sodium beam was collimated by a heated 3 cm wide $\times 0.6$ cm high horizontal slit, to intercept the entire F-atom spray.

The atomic reagent F was formed in a 2450 MHz, 60 W microwave discharge. Either discharged F_2, diluted in Ar or He, or discharged CF_4, pure or diluted in He, were used as the source of F atoms. The gases were supplied by the Matheson Co. The CF_4 (99.7%), He (U.H.P. 99.999%), 1% F_2/Ar mixture and 5% F_2/He mixture were used directly from the cylinder without further purification. A constant forepressure of non-corrosive gases was maintained with a Matheson model 40 vacuum regulator. For the corrosive F_2/inert gas mixture a Nupro M-4SG Monel fine metering valve was used to cut the pressure down from cylinder pressure to a range of 100–300 Torr. A Monel pressure gauge was used to measure the forepressure. The Cu tubing leading to the glass part of the gas inlet system was passivated prior to an experiment. Gas flows were measured using Tri-Flat flow meters. Flows were regulated by Fischer–Porter Teflon needle valves. Mixing of gases was done in the low pressure region, downstream of the Teflon needle valves, utilizing the matrix of gas inlet lines described previously by Woodall.[23]

Three different discharge tubes, (a), (b), and (c), were used for producing F atoms.

(a) In this configuration the tube was made entirely of quartz. It embodied two Wood's horns and right angled bends *en route* to the reaction vessel from the discharge cavity. These reduced background discharge light to less than 0.1 counts s^{-1}.

(b) An F atom discharge could also be produced in an alumina tube. The high purity alumina (99.8% Al_2O_3) was supplied by Mc Danel Refractory. The alumina was connected with Teflon Swagelok unions to two Pyrex tubes, one leading to the gas lines and the other leading via a 45° bend to the reaction vessel. Scattered light from the discharge was < 0.5 counts s^{-1}, which was acceptable.

(c) The discharge section was identical to (b) but was made entirely of quartz. Scattered light from the discharge was < 0.5 counts s^{-1}.

Prior to an experiment, the discharge tube was cleaned internally with 10% HF_{aq}. The quartz tubes and the Pyrex section of the alumina tube were coated with a solution of orthophosphoric acid in methanol in a 1 : 1 ratio, to reduce atomic recombination.

During an experiment, the end of the discharge tube was centered between 1.5 and 2 cm above the intersection of the sodium beam axis. The discharge tube was conditioned for several hours by running the F-atom discharge during the oven warmup period. Atomic F was assumed to be thermally equilibrated.[25] Possible complications due to the 7% mole fraction of $F(^2P_{1/2})$ have been ignored. The sodium oven has been described elsewhere in detail.[26,27] Nozzle diameters used in the experiments described here were 0.2, 0.28, and 0.4 mm with 0.3, 0.3, and 0.4 mm wall thicknesses, respectively. Blackbody radiation from the oven was shielded from the photomultipliers by an apron of stainless steel foil attached to the nozzle chamber.

The Na_2 reagent constituted ~ 3%–10% mole fraction in Na. The sodium was supplied by either Fischer (A.C.S.) or Alfa Ventron (A.C.S.), packed in dry nitrogen.

Oven temperature changes required in studies of the kinetics of the wing emission, were obtained by two methods. One method was to make a substantial voltage change and then resume data acquisition once the temperature had restabilized. The other approach, termed the "temperature drift" method, involved the taking of data continuously while gradually changing the temperature, through continual voltage changes.

The sodium beam was modulated with a beam flag. A manually controlled flag was used in early experiments. For most of the experiments described here, a computer controlled beam flag was used. This allowed for frequent background measurements (every 5 s if required) with a variable duty cycle governed by the importance of the background correction.

There were two channels to the detection system; the signal channel and the monitor channel. The signal channel was used for measurement of the signal at a given wavelength. The monitor channel was used for continuous measurement of the D line emission.

In the signal channel, light was focused by a 15.0 cm focal length lens onto the entrance slit of a Jarrel–Ash 1.0 m double Czerny–Turner scanning spectrometer (model 25-100) with an effective aperture ratio of 8.7. Scattered light within the spectrometer was less than 10^{-7} at 25 Å from peak and ~ 10^{-9} at 50 Å from peak as measured using a He–Ne laser.

Hence, the wings (wing intensity $I_W \sim 10^{-6}$ of the D line intensity I_D) could be observed free of scattered light from the D line.

After dispersion through the spectrometer, the light was focused onto a cooled ITT FW-130 photomultiplier tube with an S-20 response. Typical dark noise was ~ 0.7 counts s^{-1}. The signal could be immediately displayed on either a digital counter or a linear rate meter. In addition, the signal was sent to the computer's counter for computer data acquisition and analysis.

The combination of a low noise photomultiplier tube and a double monochromator allowed the measurement of weak emission ($I_W \sim 1$ count s^{-1}) in the presence of very intense emission ($I_D \sim 10^6$ counts s^{-1}) with a reasonable signal-to-noise ratio.

The monitor channel consisted of an uncooled EMI 6256S photomultiplier tube with an S-11 response. A Wratten filter cutoff wavelengths less than 4600 Å, and neutral density filters brought the count rate down to measurable levels. Further spectral filtering was not required since the D line accounted for virtually all of the emission. Monitor signal levels were in the range 1000–5000 counts s^{-1}.

The monitor channel was aligned with the optical axis of the signal channel. The monitor channel cone of sight was ~ 0.5× the signal channel cone of sight.

The data were corrected for the relative sensitivity

TABLE I. Conditions used for D line intensity calculation.

Nozzle diameter (mm)	0.4
T_O [oven body temperature (K)]	846
T_N [oven nozzle temperature (K)]	962
P_{Na} ahead of nozzle (Torr)	17
P_{Na_2} ahead of nozzle (Torr)	0.4
CF_4 flow (μ mol s^{-1})	0.4
He flow (μ mol s^{-1})	8
I_D (counts s^{-1}; observed)	2.4×10^4

of the detection system as a function of wavelength by comparison of the measured signal from an 800 °C blackbody with that expected from theory.

III. RESULTS AND DISCUSSION

Emission by electronically excited sodium atoms from the $3\,^2P$ states (Na*) to the ground state yields the D lines of sodium. The unresolved D lines dominated the observed visible spectrum when uncollimated beams of F atoms and Na_2 were mixed in the reaction vessel at reagent pressures of $\sim 10^{-5}$ Torr. For the experiments in which emission from the transition state $FNaNa^{\dagger *}$ was studied, total D line emission ranged from $\sim 4\times10^5$ to $\sim 5\times10^6$ counts s^{-1}. The following arguments showed that the reaction

$$F + Na_2 \rightarrow NaF + Na^*(3\,^2P) \qquad (1)$$

was the source of the D line emission.

First we compared the measured intensity of the D line I_D, with that anticipated assuming reation (1) to be the source of $Na^*(3\,^2P)$. The requisite numbers are to be found in Table I; the parameters required were the rate constant for reaction (1) k_1 the reagent number densities (Appendix A), the detection efficiency, and the volume of observation. The calculation is set out in Appendix B. The calculated value was $I_D = 1.5\times10^6$ counts s^{-1}, in good agreement with the measured value of 2.4×10^6 counts s^{-1}.

Next we identify the reactants responsible for forming $Na^*(3\,^2P)$. The dependence of the D line intensity I_D on $[Na_2]$ was determined by overheating the nozzle with a constant oven body temperature. In this way the $[Na_2]$ could be decreased while retaining a constant [Na].[28] The D line signal was found to be halved when the nozzle temperature was increased from 1020 to 1122 K while the oven body temperature was constant at 926 K. The change in $[Na_2]$ was calculated assuming either an equilibrium dimer mole fraction[29] or a supersonic expansion.[30] These approximate calculations yielded values of the decrease in $[Na_2]$ by factors of 2.2 and 1.5, respectively, in agreement with the observed factor of 2. This indicated that Na_2 was one of the reagents responsible for the D line emission.

Higher polymers, such as Na_3, could not have been responsible for the D line emission since the concentrations of such species were too small. The ratio $[Na_3]/[Na_2]$ has been measured to be about 0.01–0.03 under conditions similar to those used in the experiments described here.[31,32] The low value of $[Na_3]$ indicates that any hypothetical reaction of Na_3 or higher polymers would have to be impossibly fast to contribute to I_D.

Atomic F was shown to be the other reagent in the reaction responsible for the D line emission. Consumption of F by H_2, added to the F atom flow through a sidearm 3 cm upstream from the end of the discharge tube, decreased I_D to about 3%. Since removal of F atoms markedly decreased the D line emission, it appears that atomic F was one of the reagents involved in the reaction leading to D line emission.

When the flow of discharged F_2 was reduced by a factor of 2, the value of I_D decreased by the same factor, again indicating that the D line emission was due to F atoms.

It was possible that two other mechanisms could have led to some D line emission in this system. These were mechanism A[14,33]

$$F + Na_2 \rightarrow NaF^{\dagger} + Na(3\,^2S)\ , \qquad (2)$$

$$NaF^{\dagger} + Na \rightarrow NaF + Na^*(3\,^2P)\ , \qquad (3)$$

and mechanism B[33,34]

$$Na + F_2 \rightarrow NaF^{\dagger} + F\ , \qquad (4)$$

$$NaF^{\dagger} + Na \rightarrow NaF + Na^*(3\,^2P)\ . \qquad (3)$$

However, the involvement of these alternative processes was shown to be small.[27]

Mechanism B, which depends only on Na, could not have been significant since (in the experiment discussed above) overheating of the nozzle decreased I_D by approximately the same factor as the calculated decrease in $[Na_2]$. With the discharge off and F_2 flowing, mechanism B was the principal source of D line emission. Measurement of the intensity under these conditions showed that the contribution to I_D from mechanism B under normal operating conditions amounted to about 10%.

The yield of Na* from mechanism A could be calculated from the measured importance of mechanism B (discharge off). Substitution of the values of [F] and $[Na_2]$ with the discharge on, in place of [Na] and $[F_2]$, led to a contribution of 5% to I_D from mechanism A.

We conclude that the principal source of the observed D line emission was reaction (1). Hence, the D line intensity provides a measure of the product of concentrations $[F][Na_2]$.

Weak emission ($\sim 10^{-6} I_D$) was observed at both shorter wavelengths (blue wing) and longer wavelengths (red wing) than that of the D line. These wings are shown in Fig. 2. Evidence from calculation and experiment, presented below, shows that the wing emission was chemiluminescence from the transition state $FNaNa^{\dagger *}$ in reaction (1).

First, the intensity of the wing emission was near to

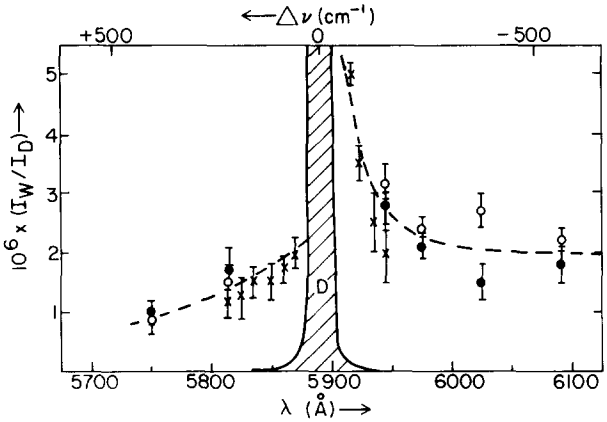

FIG. 2. Observed emission ("wings") to either side of the D line. Discharged CF_4 is the source of the atomic reagent F in the reaction $F + Na_2 \rightarrow NaF + Na^*$. Points designated ● at 5817 and 5977 Å were taken from the slopes of plots of I_W as a function of I_D in Ref. 10. Points designated ● at other wavelengths were measured under the conditions of Table I (see also Ref. 10). Error bars represent one standard deviation. Points designated ○ were obtained from the intercepts of plots of I_W/I_D as a function of I_D. Error bars represent one standard deviation in the intercepts of linear least squares fits to the plots. Conditions are given in Table II. Points designated by × were taken from a spectral scan of I_W/I_D. Error bars represent one standard deviation. Conditions for these points are given in Table II. The dashed curves are estimates of the red wing and the blue wing profiles.

that expected from transition state emission. The intensity of transition state emission was calculated in a $3D$ trajectory study performed in this laboratory.[3] It was found that I_W was about $5\times10^{-7}\, I_D$ at a single wavelength in the spectral region observed experimentally. The resolution was 8.8 Å, as in the experiments. The observed value of I_W/I_D as seen in Fig. 2 was $\sim 1-2 \times 10^{-6}$. The agreement is satisfactory considering that the trajectory study was performed using guessed potential energy surfaces that merely matched the exothermicities.

The spectral shape (i.e., wing intensity as a function of wavelength) is a second piece of evidence indicating that the wings were due to $FNaNa^{\ddagger}*$ emission. Three separate measurements of the wing are shown in Fig. 2. Each shows a decline in I_W/I_D as $|\Delta\nu|$ increases ($\Delta\nu$ is the distance in cm^{-1} away from the D line peak wave number).

This characteristic was expected of transition state emission because the emission nearest to the D line must arise from configurations in which Na* is far from NaF. Since potentials are likely to be smoothly varying functions, the change in frequency of the emission with increasing product separation will be smaller at these large separations. Therefore, in the classical Franck–Condon approximation, intensity is built up at the frequencies near the asymptotic potential difference. Another factor which is likely to contribute to the fall in intensity away from the D line is the diminished probability of finding the products a short distance apart, corresponding to the extreme wings.

The above considerations were based upon the quasi-static theory of "far" and "extreme" wing broadening.[13] Many examples of far and extreme wing broadening of M* (M is an alkali metal) by inert gases have shown a fall in intensity away from the D line.[12] This feature was also found in the wings generated in the trajectory study by Polanyi and Wolf.[3]

Since both the intensity and the shape of the observed wings was in accord with that expected of transition state emission, it was plausible that the observed wings were due to emission from $FNaNa^{\ddagger}*$.

Several other sources of emission could also yield wings which would fall off to either side of the D line. Their intensities might, by chance, be in the range expected for transition state emission. Two such possibilities which can readily be calculated are Lorentz natural lifetime broadening and Doppler broadening. These are calculated in Appendix C. It is shown that that Doppler broadening is entirely negligible at the wavelengths observed experimentally. Emission due to Lorentz natural lifetime broadening is less than 5% of the observed wings further than 70 Å from the D line. (It should be noted, moreover, that the dependence on wavelength of the observed wing emission is not Lorentzian.) For wavelengths closer than about 50 Å from the D line in the blue wing the Lorentz wings become significant. Correction for this Lorentz contribution tends to flatten out the rise in the near blue wing, though leaving a significant rise from ~5750–5813 Å. The rise of the red wing is insignificantly affected.

Another type of broadening which could have given the shape of the wings observed experimentally is pressure broadening by a gas in the reaction vessel. This will be called secondary broadening to distinguish it from the broadening of Na* emission due to the reactive encounter.

Secondary broadening would occur following the chemical formation of Na*. At the low densities in the reaction zone in these experiments {expressed in particles/cm^3 $[Na]\sim 1\times10^{12}$, $[Na_2]\sim 2\times10^{10}$, $[CF_4]\sim 4\times10^{11}$, $[F]\sim 8\times10^{11}$, and $[He]\sim 4\times10^{12}$ (Appendix A)} and in the absence of very substantial trapping, only a negligible fraction of the Na* formed chemically could have collided with another gas atom or molecule before being removed by radiation. This is borne out by the calculations of Appendix D. In the absence of trapping, it is shown in Appendix D that the total contribution of secondary broadening to the wing would have been $9\times10^{-10}\, I_D$ at a wavelength of ~6000 Å for the conditions of Table I. The observed wing intensity at this wavelength was $\sim 2\times10^{-6}\, I_D$.

Secondary broadening could have been enhanced due to radiation trapping and self-absorption of the $Na^*(3\,^2P)$ emission. This was not, however, found to be the case.

The extents of both radiation trapping and self-absorption in our experimental system are estimated in Appendix E. Experiment and calculation indicated that both effects were negligible. This was primarily due to the fact that the Na* formed in the $F + Na_2$ reaction

TABLE II. Conditions for Figs. 3(a)–3(g) and spectral trace denoted X in Fig. 2. Columns 1–4 give conditions for the points at different oven temperatures recorded in each of Figs. 3(a)–3(d), 3(f), and 3(g). The range of conditions in column 5 refers to the temperature drift experiment of Fig. 3(e). Column 6 gives experimental conditions for the continuous spectral trace denoted by X in Fig. 2.

$10^{-6}\ I_D$ (counts s^{-1})	0.71	1.24	2.15	3.09	0.8–3.0	0.6
Nozzle diameter (mm)	0.20	0.20	0.20	0.20	0.20	0.28
T_O [oven body temp. (K)]	936	955	972	991	927–981	931
T_N [oven nozzle temp. (K)]	1088	1110	1115	1150	1042–1086	1000
P_{Na} ahead of nozzle (Torr)	~70	~93	~115	~147	~60–124	~62
P_{Na_2} ahead of nozzle (Torr)	~2.2	~3.0	~4.0	~5.7	~2.4–6.8	~3.7
Na flow (μ mol s^{-1})	~7.4	~9.4	~11.3	~16.6	~6.5–12.6	~13.6
Na_2 flow (μ mol s^{-1})	~0.42	~0.58	~0.76	~1.08	~0.4–1.2	~0.6
CF_4 flow (μ mol s^{-1})	2.8	2.8	2.8	2.8	1.8	0.75
He flow (μ mol s^{-1})	35.4	35.4	35.4	35.4	35.4	0

had substantial Doppler breadth along the spectrometer's optical axis, whereas the absorbing Na gas moved preferentially along a line perpendicular to the optical axis. Hence, the absorbers exhibited only a very narrow absorption.

Since trapping and self-absorption were negligible, the effects of secondary broadening could be completely neglected.

An important feature of the wing emission was that the kinetics was characteristic of emission from $FNaNa^{\ddagger *}$. It was established above that I_D was due to reaction (1). Hence, if I_W was due to emission from the transition state $FNaNa^{\ddagger *}$, then $I_W \propto I_D$ would hold for changes in reagent concentrations. The studies of the kinetics showed that over a range of low conditions the major component of the wing emission varied linearly with the D line. The value of I_W/I_D for this component could readily be extracted. At the high end of the I_D range, i.e., high Na_2, we observed Na_2^* banded emission. It is thought, therefore that the upward curvature in the I_W vs I_D plots at high I_D is due to the secondary process $Na^* + Na_2 - Na + Na_2^*$.

Preliminary results of the functional dependence of I_W on I_D have been previously published.[10] In the present work, the measurements of the kinetics have been extended to more wavelengths. The results are shown in Figs. 3(a)–3(g) which give I_W/I_D and also I_W as functions of I_D. The experimental conditions are given in Table II. (Absolute oven body and nozzle temperatures are approximate owing to uncertain thermal contact between the thermocouples and the oven.) The results of Figs. 3(a)–3(g) were obtained using CF_4 in an alumina discharge tube. The F atom yield was lower[35] than in a quartz tube used in the previous work[10] and hence a higher Na_2 flow was required resulting in some curvature in the plots of I_W vs I_D. The curvature is small enough that a good extrapolation can be made to $I_D = 0$. This intercept gives the value of I_W/I_D free from the contribution of $Na^* + Na_2 - Na + Na_2^*$ to the wing.

The "temperature drift" method and the earlier method of "point by point temperature variation" can be compared in Figs. 3(d) and 3(e) (both at the same wavelength in the wing). In Fig. 3(d), the intercept is 2.4 ± 0.2, whereas in Fig. 3(e) it is 2.5 ± 0.2. Evidently, the two methods are in good agreement. Hence the temperature drift method was used with confidence for the studies of the kinetics presented later in this paper using discharged F_2 as the source of F atoms.

The values of I_W/I_D obtained from the extrapolations of the I_W/I_D plots of Figs. 3(a)–3(g) are shown in Fig. 2 as open circles. The closed circles in Fig. 2 are taken from Arrowsmith *et al.*[10] The agreement is good, except at 6036 Å. There was no apparent systematic reason for the deviation at this wavelength. Error bars were based on the standard deviation in the mean of a Poisson distribution of counts.[36]

As noted above, nonlinearity in the I_W/I_D plots was due to Na_2^* emission, observed as a banded spectrum at higher reagent flows.[37] The Na_2^* emission arose from the reaction[38,39]

$$Na^*(3\,^2P) + Na_2(^1\Sigma_g^+) - Na(3\,^2S) + Na_2^*(^1\Sigma_u^+) \ .$$

Hence, this emission was second order in I_D and the wing emission was extracted by extrapolation to $I_D = 0$ in the I_W/I_D plots. The wavelengths at which I_W was measured were in the "valleys" between the Na_2^* "peaks" to minimize the Na_2^* contributions.

A check was made for contributions to the wings from secondary processes involving atomic F. This was done by varying the CF_4 flow while keeping $[Na_2]$ constant and measuring the change in I_W with the variation of I_D. In this experiment I_D acted as a measure of the relative values of [F]. The results are shown in Figs. 4(a) and 4(b). The measurements were made at the wavelengths 5817 Å (blue wing) and 5977 Å (red wing). The experimental conditions are given in Table III. It was found that I_W/I_D was constant with change in [F], to within the experimental error. The limiting values of I_W/I_D as $I_D - 0$ in Figs. 4(a) and 4(b) were 2.60 ± 0.25 at at 5977 Å and 2.07 ± 0.15 at 5817 Å. Uncertainties were

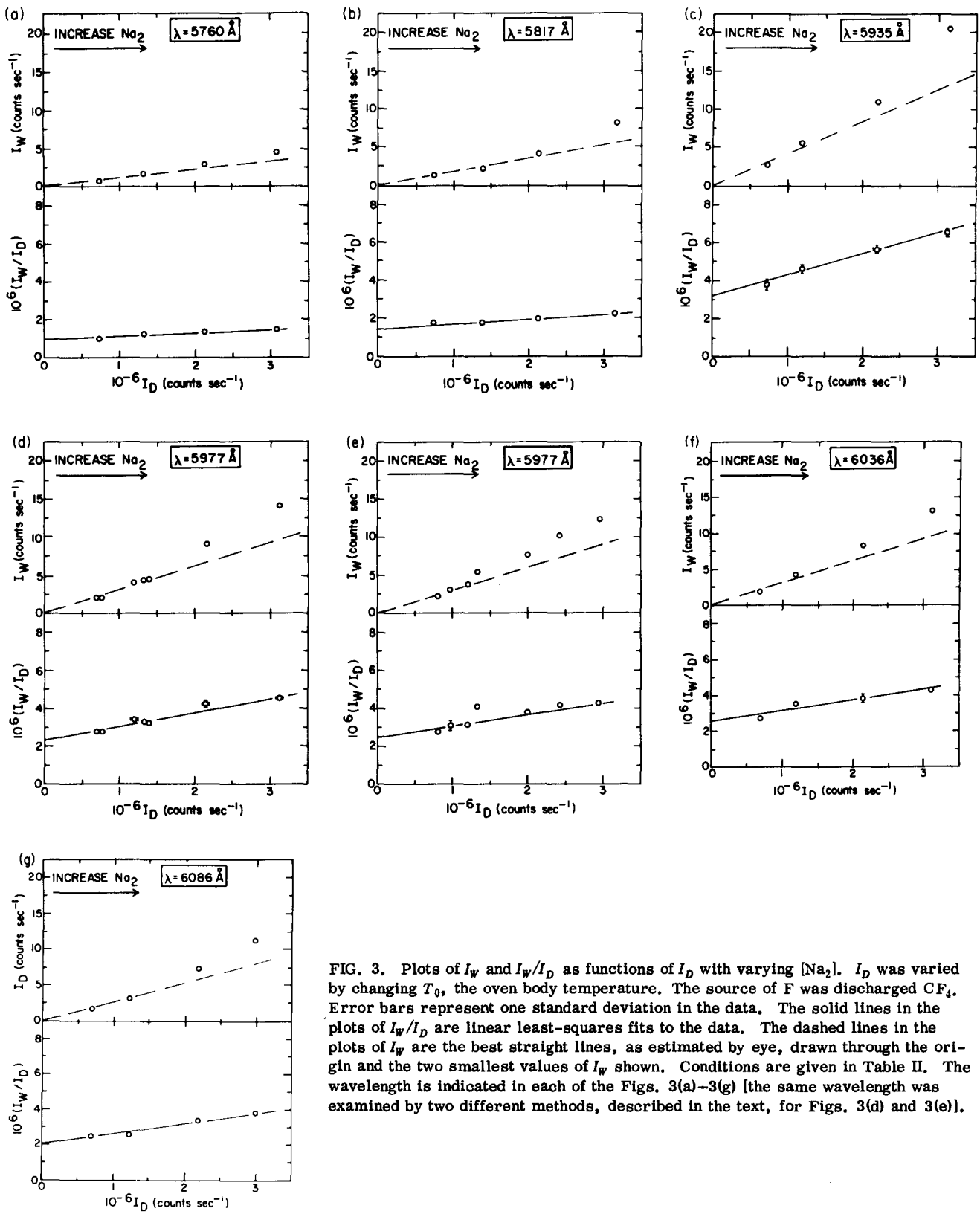

FIG. 3. Plots of I_W and I_W/I_D as functions of I_D with varying $[Na_2]$. I_D was varied by changing T_0, the oven body temperature. The source of F was discharged CF_4. Error bars represent one standard deviation in the data. The solid lines in the plots of I_W/I_D are linear least-squares fits to the data. The dashed lines in the plots of I_W are the best straight lines, as estimated by eye, drawn through the origin and the two smallest values of I_W shown. Conditions are given in Table II. The wavelength is indicated in each of the Figs. 3(a)–3(g) [the same wavelength was examined by two different methods, described in the text, for Figs. 3(d) and 3(e)].

estimated from a least-squares fit to the data.

These values for I_W/I_D can be compared to the average of the values of I_W/I_D given in Fig. 2. At 5977 Å the average value is 2.3×10^{-6} and at 5817 Å the average is 1.5×10^{-6}. Thus the results obtained by varying [F] compared favorably with the results obtained by varying $[Na_2]$.

The wing intensities represented by the symbol X in Fig. 2 were the results of a continuous spectral trace of the wings (in contrast to integration of signal at

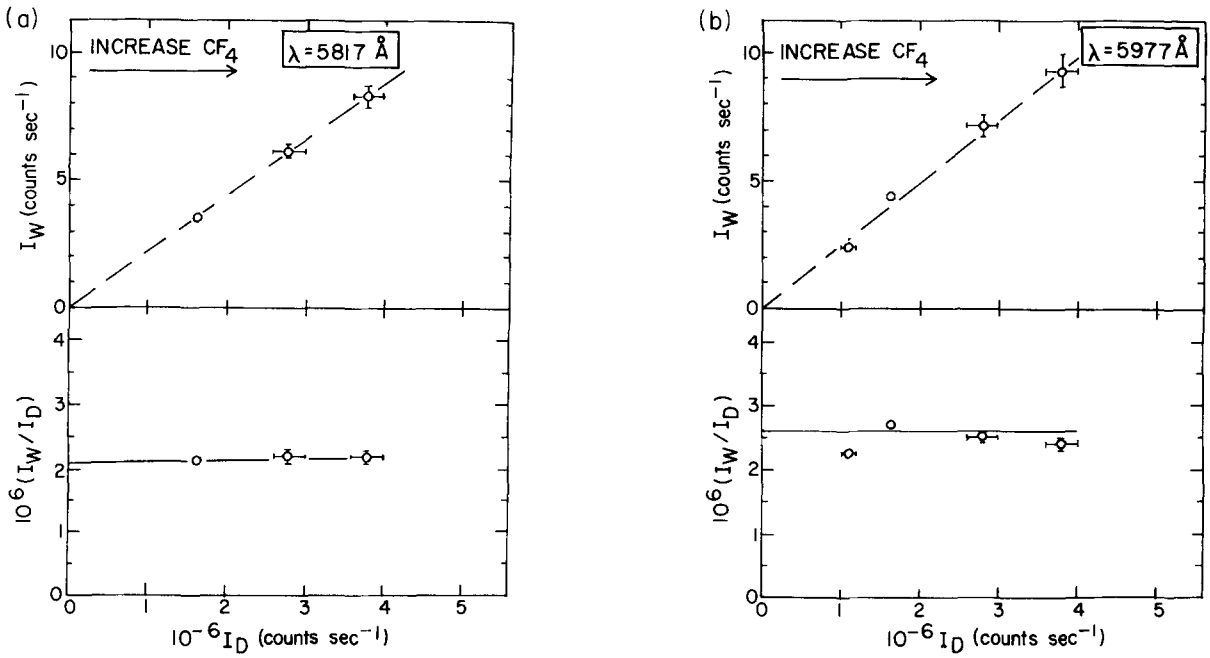

FIG. 4. Plots of I_W and I_W/I_D as functions of I_D with varying CF_4 flow (varying [F]). The dashed line in the plot of I_W is the best straight line through the origin. The solid line in the I_W/I_D plot is a linear least-squares fit to the data. Error bars represent one standard deviation in the data. Conditions are given in Table III. Figures 4(a) and (b) are recorded at the wavelengths designated.

selected wavelengths). The conditions for this spectral trace are given in Table II. The agreement with the wing intensities obtained from the other types of measurement is good.

All the experiments described above indicate that the wings arise from the intermediate $FNaNa^{\ddagger}*$.

Since this is a novel proposal we have performed experiments with the intention of looking for less probable artifacts which might affect these conclusions.

A discharge in CF_4 or a few percent CF_4 in He gives rise to other products than atomic F. We have therefore performed experiments using a few percent elemental F_2 in excess He or Ar as the source of F. The results using discharged F_2 supported those obtained using discharged CF_4.

Kinetic studies were performed, with discharged F_2, in which $[Na_2]$ was varied, and also [F] was varied. The results are to be found in Figs. 5–7. The experimental conditions are given in Table IV.

Figures 5(a) and 5(b) differ in showing blue wing and red wing wavelengths; similarly for Figs. 6(a) and 6(b), and Figs. 7(a) and 7(b). Figures 5(a) and 5(b) were obtained by varying the oven body temperature, i.e., the total flow of Na and Na_2. Figures 6(a) and 6(b) give results from variation in the nozzle temperature, i.e., changing almost exclusively the Na_2 flow. Figures 7(a) and 7(b) resemble Figs. 5(a) and 5(b) in that the oven body temperature was the variable, but differed in using one half the flow of F_2, i.e., roughly one-half the flow of F.

Figures 5 and 6, using discharged F_2 as the source

TABLE III. Conditions for the data of Figs. 4(a) and 4(b).

$10^{-6} I_D$ (counts s^{-1})	1.2	1.7	2.8	3.7
Nozzle diameter (mm)	0.45	0.45	0.45	0.45
T_O [oven body temp. (K)]	860	860	860	860
T_N [oven nozzle temp. (K)]	981	981	981	981
P_{Na} ahead of nozzle (Torr)	~22	~22	~22	~22
P_{Na_2} ahead of nozzle (Torr)	~0.57	~0.57	~0.57	~0.57
Na flow (μ mol s^{-1})	~13	~13	~13	~13
Na_2 flow (μ mol s^{-1})	~0.56	~0.56	~0.56	~0.56
CF_4 flow (μ mol s^{-1})	0.1	0.7	1.1	2.0
He flow (μ mol s^{-1})	8.0	8.0	9.2	9.2

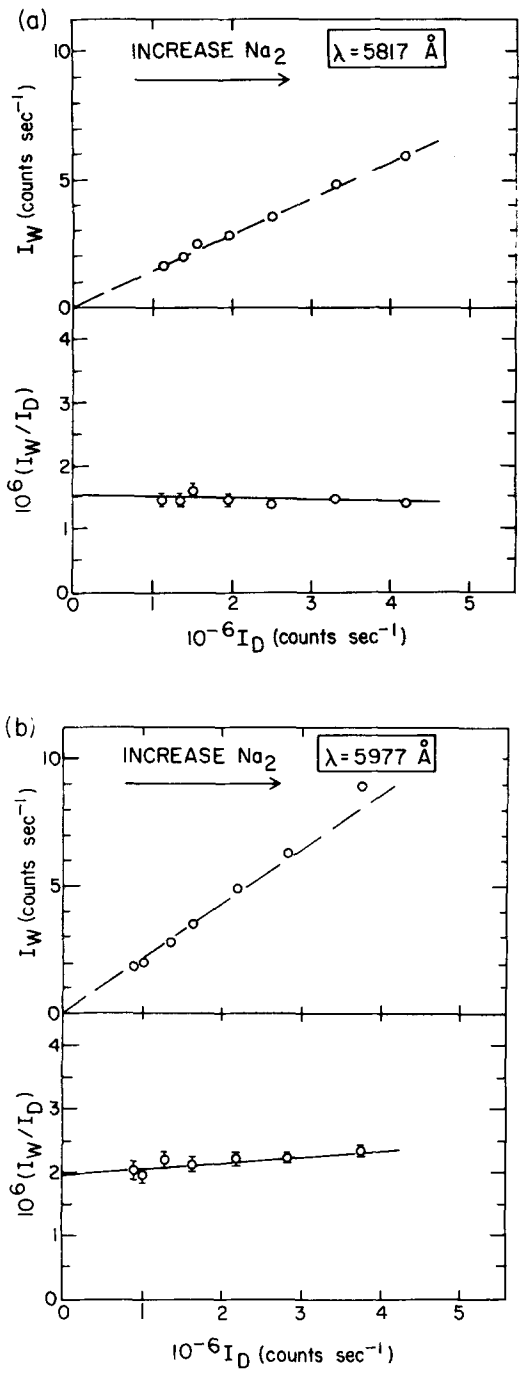

FIG. 5. Plots of I_W and I_W/I_D as functions of I_D with varying [Na_2]. The source of F was discharged F_2. I_D was varied by changing T_O, the oven body temperature. Error bars are one standard deviation. Conditions are given in Table IV. The solid lines in the plots of I_w/I_D as a function of I_D are linear least-squares fits to the data (the same is true of Figs. 6 and 7). The dashed lines in the plots of I_W as a function of I_D are the best straight lines (estimated by eye) through the origin. Figures 5(a) and 5(b) are for the designated wavelengths.

of F, showed an improved linearity of I_W with I_D as compared with the discharged CF_4. This almost certainly stems from the fact that the larger F atom flow from F_2—which we confirmed by comparison with CF_4—allowed us to use a lower range of Na_2 flows. (As already indicated, oven temperatures for the three batches of experiments that gave the data for Figs. 3, 4, and all of Figs. 5–7, cannot be compared with each other dependably, since each reassembly of the oven and thermocouples led to somewhat different temperature gradients between thermocouples and oven.) In collecting the data for Fig. 7, at reduced F, the Na_2 flow had to be increased (Table IV, column 3). The expected slight upward deviation in I_W vs I_D is evident in this figure, due to a contribution from $Na^* + Na_2 \rightarrow Na + Na_2^*$ secondary emission at the higher Na_2 flow.

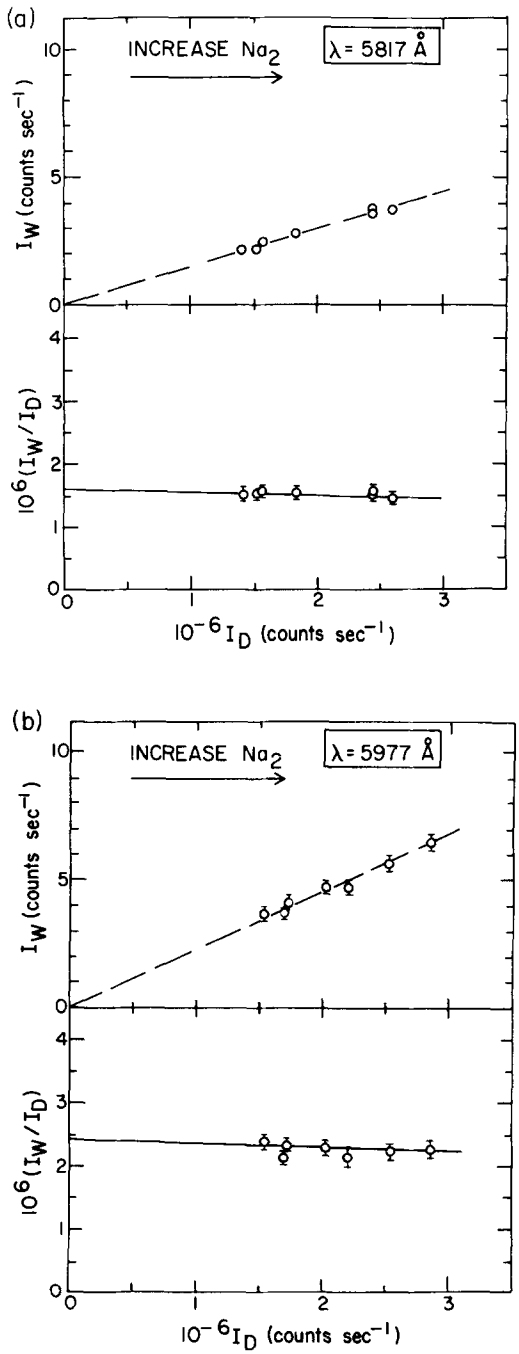

FIG. 6. Plots of I_W and I_W/I_D as functions of I_D, with varying [Na_2]. The source of F was discharged F_2. I_D was varied by overheating the nozzle. Error bars are one standard deviation. Conditions are given in Table IV. Figures 6(a) and 6(b) are for the designated wavelengths.

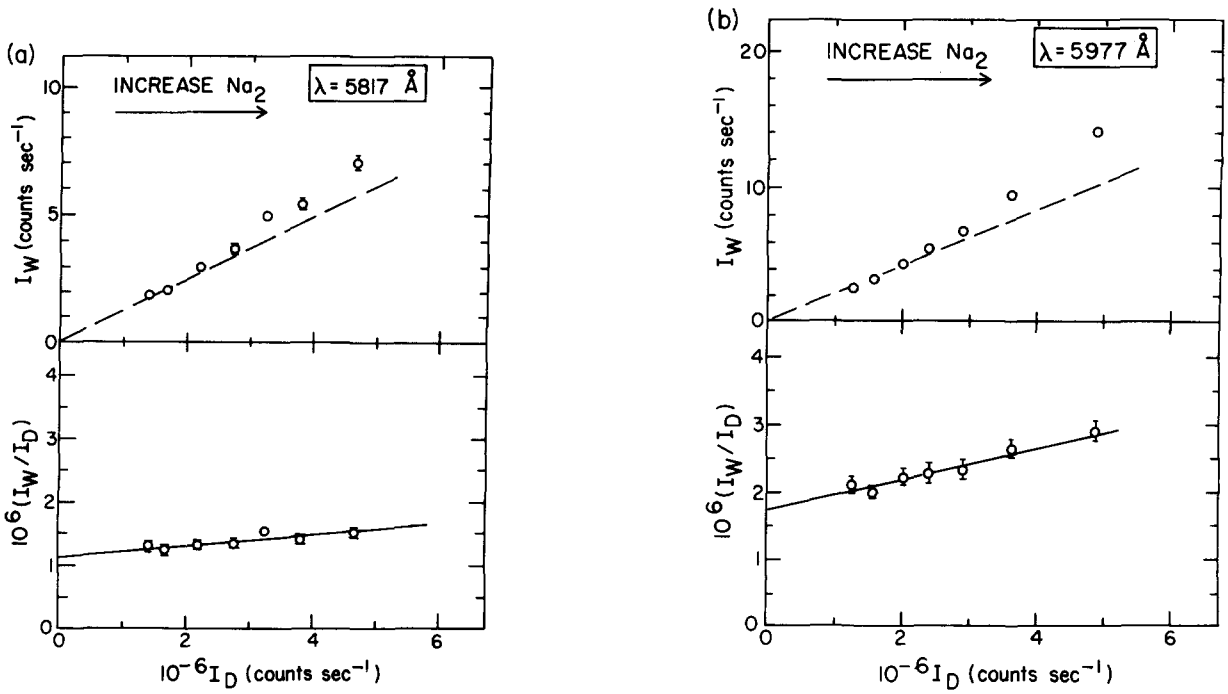

FIG. 7. Plots of I_W and I_W/I_D as functions of I_D, with varying [Na_2]. The source of F was discharged F_2. The flow of discharged F_2 was a factor of 2 lower than that of Fig. 5. I_D was varied by chainging T_O, the oven body temperature. Error bars are one standard deviation. Conditions are given in Table IV. Figures 7(a) and 7(b) are for the designated wavelengths.

The general conclusion is that, as expected for transition state emission, the wing intensity increases linearly with the D line intensity. Substitution of discharged F_2 for discharged CF_4 does not affect this finding.

In the limit of low flows as $I_D \to 0$, in Figs. 5(a)–7(a) and also in Figs. 5(b)–7(b) the intercepts should be the same (for each group). Within the considerable experimental error, this is the case.

The average values of these intercepts are shown as triangles in Fig. 8. All the points on this figure were obtained in the (relatively small number of) experiments employing discharged F_2 as the source of F. The black squares were obtained in a preliminary experiment with discharged F_2, performed on one day. The experimental conditions closely approximated those recorded in Table I. The open squares give average intensity ratios for three experiments performed sequentially at two different oven temperatures (approximately 2.5×change in Na_2 flow) and at two F_2 flows (approximately 2×change in flow). The broken line sketched in Fig. 2, embodying the bulk of our experiments, which were performed using CF_4 as the source of F falls within the shaded area of Fig. 8 obtained using F_2 as the source of F.

The sources of the scatter in the points recorded in Figs. 2 and 8 are only partially understood. The points record the relative intensities of two signals I_W and I_D, differing by ~ 10^6. In earlier experiments (black

TABLE IV. Conditions for data of Figs. 5–7. Columns 1, 2, and 3 give the ranges of conditions for Figs. 5, 6, and 7, respectively.

10^{-6} I_D (counts s^{-1})	0.9–4.2	2.8–1.5	1.3–4.8
Nozzle diameter (mm)	0.28	0.28	0.28
T_O [oven body temp. (K)]	890–941	928	919–977
T_N [oven nozzle temp. (K)]	980–1010	1012–1122	1005–1062
P_{Na} ahead of nozzle (Torr)	~ 35–71	~ 62–66	~ 55–116
P_{Na_2} ahead of nozzle (Torr)	~ 1.4–4.5	~ 3.5–1.5	~ 2.6–7.1
Na flow (μ mol s^{-1})	~ 8–16	~ 15	~ 22–24
Na_2 flow (μ mol s^{-1})	~ 0.5–1.7	~ 1.2–0.7	~ 0.5–1.4
F_2 flow (μ mol s^{-1})	1.75	1.7	0.8
He flow (μ mol s^{-1})	35	35	32

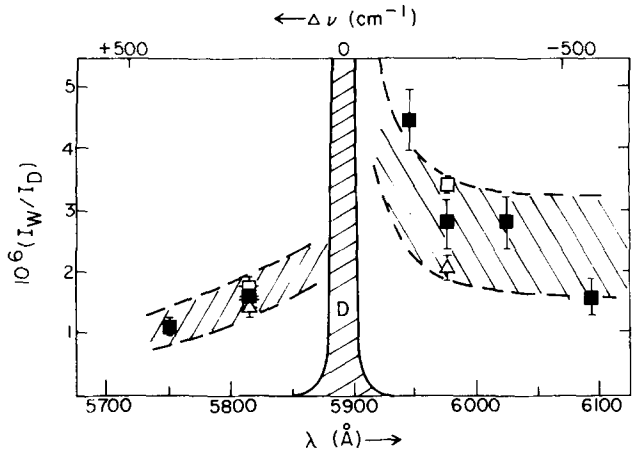

FIG. 8. Wings of the D line with discharged F_2 as the source of the atomic reagent F. Points designated by ■ were taken under conditions similar to those in Table I. Error bars represent two standard deviations. Points designated by □ give average intensity ratios for three experiments performed sequentially at two different oven temperatures and two F_2 flows (see the text). The error bars represent one standard deviation in the mean. Points designated by Δ are averages of data points taken under conditions of Table IV. Error bars represent one standard deviation in the mean. The shapes of the dashed boundaries are parallel to the shape of the dashed curve estimated in Fig. 2. The boundaries were set according to the maximum scatter in the data points at 5817 Å (blue wing) and 5977 Å (red wing). The dashed curves of Fig. 2 fall within these boundaries.

circles in Fig. 2, and black squares in Fig. 8) I_W and I_D were recorded sequentially on the same device—the double monochromator. Since fluctuations in I_D could occur between successive readings, a separate optical channel, consisting of a photomultiplier viewing the reaction zone from the opposite end of the vessel, was used for continual monitoring. Some error may stem from the difference in the regions of emission being sampled by the I_W and the I_D channels, though checks of I_D continued to be made at intervals through the I_W optical channel. A fuller understanding of the systematic errors will have to await a reconfiguring of the apparatus, now under way.

In what follows we shall discuss, in turn, the possible contribution of (a) Na_2^* (electronically excited Na_2) (b) NaF*, (c) impurities generated in the microwave discharge, and (d) luminescent surface reaction.

(a) Emission from $Na_2^*(A\,^1\Sigma_u^+)$. In experiments performed at somewhat higher flows of sodium than the highest used in the experiments recorded in Figs. 2–8, a banded emission was observed in the region of the blue and (especially) the red wings that was clearly due to Na_2^*.[37–39] This emission arose from the secondary process of electronic-to-electronic (E–E) energy transfer, $Na^* + Na_2 \rightarrow Na + Na_2^*$, alluded to above. The linearity of the plots of I_W vs I_D recorded in Figs. 3, 5, 6, and 7 shows that the contribution of this process to the wing emission in the low flow range was negligible.

However, there could possibly be a primary process (not involving Na*) giving rise to Na_2^*. Gole and coworkers have found evidence for a reaction of atomic halogens with Na_3 of the type

$$F + Na_3 \rightarrow NaF + Na_2^*$$

(the specific case of F was not studied[40]). The emission consisted of various band systems including $A \rightarrow X$.

There are several reasons for believing that this reaction is not the cause of the wing emission recorded in the present work. In the first place it would be a coincidence if the emission from Na_2^* formed in the $F + Na_3$ reaction centered on the Na D line wavelength. Second, there is no evidence for Na_2^* band structure under the conditions used to record the wings; these bands do, however, appear at higher Na_2 flows as a result of a secondary process, i.e., in the more nearly quadratic region of I_W vs I_D where $Na^* + Na_2 \rightarrow Na + Na_2^*$ contributes significantly. Third, diminution in the wing emission consequent on overheating the nozzle section of the oven accords well with the bond dissociation energy of Na_2 [D(Na–Na) = 17.0 kcal mol^{-1}[41]] and less well with that for Na_3 [$D(Na_2$–Na) = 8.4 kcal mol^{-1}[42,43]]. Finally we note that varying oven temperature [Figs. 5(a), and 5(b)] or changing the nozzle temperature [Figs. 6(a), and 6(b)] will alter the ratio $[Na_3]/[Na_2]$, yet the ratio of wing intensity to D line (which depends on $[Na_2]$) remains constant to within experimental error.

(b) Emission from NaF*. The lowest excited states of NaF[44] could, in principle, give rise to emission in the region of the wings. However, this is unlikely in view of the failure to observe NaF* emission in studies of high pressure diffusion flames of sodium plus fluorine,[45] and in a beam-gas study of $Na_2 + X_2$ ($X_2 = F_2$, Cl_2, Br_2) which yielded NaCl* and NaBr*.[34]

Since we are dealing, in the wing, with a feeble emission we have, nonetheless, considered whether the kinetics are in accord with any possible source of NaF*. Since the emission centers on the D line the most likely mechanism for forming NaF* would be E–E transfer; $Na^* + NaF \rightarrow Na + NaF^*$. This is disqualified since it would require that the wing intensity be quadratic with the D line emission.

A further possible mechanism might be radiative recombination $Na + F \rightarrow NaF^*$. This process, however, depends only on Na whereas [see Figs. 6(a) and (b)] the wing and D line emissions depend on the Na_2 concentration.

Finally, there is the bimolecular mechanism $Na_2 + F_2 \rightarrow NaF^* + NaF$, analogous to that involved in NaCl* and NaBr* formation. It would be necessary that, by chance, this give rise to emission centered on the D line. Though this is improbable we have made an estimate of the maximum contribution to the observed wings due to reactions with residual F_2 coming from the discharge tube, so as to set an upper limit on the contribution from the $Na_2 + F_2 \rightarrow NaF^* + NaF$ reaction.

For this estimate it was first necessary to ascertain the decrease in $[F_2]$ in the reaction zone upon turning on the discharge in a 5% F_2 + 95% He inflow. D line emission $I_D(F_2)$ was obtained from Na + F_2, as already noted. Excess H_2 was added in the last 3 cm of the

$F + F_2$ inlet to remove all F, and $I_D(F_2)$ was then used as a measure of F_2. This was done with the discharge on and off, to get a value for the decrease in $[F_2]$ when the discharge was on. The decrease was found to be by a factor of 8.

The contribution of all processes involving F_2 to the observed wing in experiments with F coming from discharged F_2 could then be calculated to be $\frac{1}{8}$ of the count rate obtained with the discharge off. This amounted to a 20% contribution at 5977 Å and 11% at 5817 Å. These represent upper bounds to the total contribution to the observed wings from processes involving F_2, since they were measured under conditions corresponding to the largest residual F_2 inflow, namely F_2 in the discharge and alumina tubing (the latter gives a reduced percentage dissociation[35]).

The contribution of NaF* to the observed wings is, therefore, believed to have been unimportant.

(c) Emission from impurities generated in the microwave discharge.

A trace impurity entering the reaction zone from the microwave discharge in F_2, could be HF formed by reaction of F with water adsorbed at the wall.[46] The 6-1 band of $HF^\dagger$ emits in the spectral region of the wings.[47] Engelke[48] observed the visible overtone emission from $HF^\dagger$ formed in the V → V transfer

$$NaF^\dagger + HF \rightarrow NaF + HF^\dagger \ .$$

In addition to HF formed in the discharge, there was a 0.2% impurity of HF (Matheson report G-115) in the F_2, which had been used without further purification.

The results indicated, however, that $HF^\dagger$ did not contribute significantly to the experimentally measured wings. First, the V–V transfer process $NaF^\dagger + HF$ is second order in [F], whereas the observed wings were first order in [F]. Furthermore, no $HF^\dagger$ emission was observed in spectral scans of the blue wing taken at high reagent flows. If present, the 6-1 band would have been easy to identify (see, e.g., Ref. 47).

Other impurities from the F atom discharge besides HF were ruled out as sources of the wing emission. Inert gas metastables could be eliminated since the points designated by X in Fig. 2 were obtained without any inert gas in the discharge. The wings were observed when CF_4, discharged in either an alumina or quartz tube was the source of the atomic reagent F. The wings were also observed when discharged F_2 was used as the source of F atoms. The only impurity worth consideration and common to all of the different F atom sources was F_2. The contributions to the wings from processes involving F_2 were discussed above in connection with NaF*. It was found that processes involving F_2 contributed at most, 10%–20% of the observed wings.

(d) Emission due to surface reaction. Continuum emission has been observed previously in reactions of halogens (Cl_2, Br_2, and I_2) with a sodium surface.[24] In the experiments described here no sodium covered surfaces fell within the cone of sight of the spectrometer. Moreover, the intensity of emission from a sodium surface would depend almost totally on the flow of Na and only very weakly on the flow of Na_2 because of the small dimer mole fraction in the "beam" (~5%–10%). The results of Figs. 6(a) and 6(b) showed that $I_W \propto I_D$ with changing $[Na_2]$ and nearly constant [Na]. Therefore, these results ruled out contributions from processes involving only Na, such as reaction of F at a sodium surface.

We conclude that impurities and surface reaction made a negligible, or at most a minor, contribution to the observed wings.

The wings observed to either side of the D line bore a constant ratio to the D line with changing reagent concentrations. The wings decline in intensity to either side of the D line. The wing intensity is typically 10^{-6} ×the D line intensity, at wavelengths in the spectral region examined. The kinetics, spectral shape, and intensity of the wings are in accord with the expected properties of transition state emission from $FNaNa^\dagger*$.

IV. SPECTRAL CHARACTERISTICS OF THE WINGS

The qualitative features of the wings (Fig. 2) are as follows: (i) Both a blue wing and a red wing are observed. (ii) The intensity of the blue wing is smaller than that of the red wing. (iii) The blue wing rises steadily and gradually in intensity toward the D line. The red wing is at first almost flat (> 50 Å away from the D line), and then rises steeply toward the D line.

One simple interpretation of the blue and red wings of $FNaNa^\dagger*$ is that each wing arises from its own excited state hypersurface.

This is proposed in view of previous theoretical studies on the potentials for the reactions of halogen atoms with alkali metal dimers. (This discussion of $FNaNa^\dagger*$ is restricted to collinear potentials.) Collinear cuts in the exit channels of the ground and excited state surfaces, with fixed FLi separations, were generated by Balint-Kurti and Karplus[19,20] using the orthogonal Moffit method. Analogous potential energy curves were generated by Struve for ClNaNa[21] and BrKK[17] using the semiempirical pseudopotential method. Qualitative potential curves for $F + Na_2$ are shown in Fig. 9. These curves were based roughly on the FLiLi potentials of Balint-Kurti.[19,20]

One similarity in both of the theoretical studies mentioned above was that the potential energy difference spectrum between the $^2\Pi$ state [leading to $M^*(^2P)$] and $^2\Sigma^+$ ground state [leading to $M(^2S)$] corresponded to a blue wing, i.e., the potential energy differences were all greater than the asymptotic difference. In addition, the potential energy difference spectrum between the excited $^2\Sigma^+$ state [also leading to $M^*(^2P)$] and the $^2\Sigma^+$ ground state [leading to $M(^2S)$] correspond to a red wing.

Experimentally, the blue wing was about a factor of 2 smaller than the red wing. This could be explained by the fact that the $^2\Sigma^+$ excited state showed a much longer range interaction than either the $^2\Pi$ excited state or the $^2\Sigma^+$ ground state for FLiLi. A longer range interaction implies a larger wing intensity. (If the asymptote is

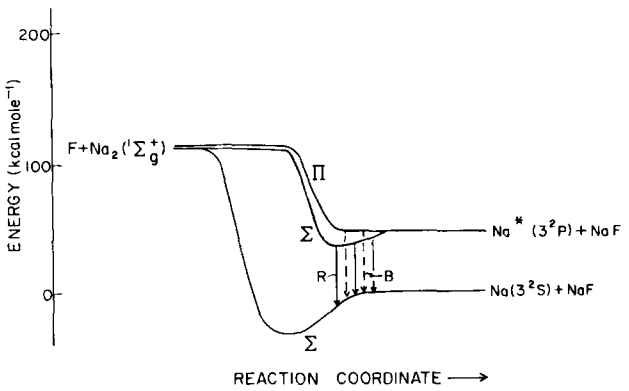

FIG. 9. Qualitative potential curves for collinear $F + Na_2$ reactions. The curves, based on Balint-Kurti's calculated curves, are drawn in the adiabatic representation. The solid arrows designated by R denote transitions yielding red wing emission. The dashed arrows designated B denote transitions yielding blue wing emission.

approached more slowly, $d\nu/dR$ is smaller, enhancing the intensity, and additionally there is a larger probability of finding the system at separations R, that give wing emission.)

Based on Balint-Kurti's calculated curves, it appears that the blue wing of $FNaNa^{\ddagger *}$ is due mainly to the gradual increase of the $^2\Sigma^+$ ground state towards its asymptotic value; i.e., the potential energy of the separated products $Na(3\,^2S) + NaF$. This is illustrated in Fig. 9. In Balint-Kurti's calculations, the $^2\Pi$ state of FLiLi has already reached its asymptote at an Li–Li separation of about 8.5 a.u., whereas the $^2\Sigma^+$ ground state was ~2000 cm^{-1} from its asymptote at this separation (see Table VII of Chap. VI in Ref. 19).

In addition the $^2\Sigma^+$ excited state obtained in Balint-Kurti's calculations had longer range interactions than the $^2\Sigma^+$ ground state. This is also illustrated in Fig. 9. This excited states was ~8700 cm^{-1} from its asymptote at 12 a.u. Li–Li separation, whereas the ground state was only ~500 cm^{-1} from its asymptote. Thus, the longer range interactions of the $^2\Sigma^+$ excited state could account for the red wing being larger than the blue wing for $FNaNa^{\ddagger *}$.

The curves calculated by Balint-Kurti may also provide a clue to understanding the fact that the experimentally observed blue wing of $FNaNa^{\ddagger *}$ rises gradually in intensity as the D line is approached while the red wing shows a more sudden rise as the D line is approached.

It was hypothesized above that the blue wing arises mainly from the approach of one surface (the $^2\Sigma^+$ ground state) to its asymptote. Moreover, this approach ought to be relatively gradual since there is no reason for sudden changes in the slope of the collinear curve of the $^2\Sigma^+$ ground state. Thus, the blue wing should gradually increase in intensity as the D line is approached.

According to Balint-Kurti,[19] the $^2\Sigma^+$ excited state which he calculated for FLiLi undergoes an avoided crossing with a higher Σ state (not shown in Fig. 9) at internuclear separations greater than 12 a.u. The avoided crossing implies a significant decrease in the slope of the curve at separations larger than that of the avoided crossing. Therefore, $d\nu/dR$ decreases, and the intensity increases, at these larger separations. The avoided crossing in the $^2\Sigma^+$ excited state could explain the more sudden rise in I_W/I_D for the red wing as the D line is approached.

If it is assumed that the blue and red wings were each due to their own excited states, then it must be recognized that the relative intensity of the blue and red wings may also have been determined, in part, by the form of the energy release (attractive, mixed and repulsive) on the two surfaces. According to Struve[21] the excited Σ state for $Cl + Na_2$ is attractive while the Π state has about half of its exothermicity released repulsively. A more repulsive surface, for a given mass combination ($F + Na_2$ in this case), implies that a larger fraction of the exothermicity is channeled into product translation.[49,50] It was hypothesized above that reaction on the Π state yields the blue wing and reaction on the $^2\Sigma^+$ excited state yields the red wing. Thus, the lower intensity of the blue wing may also be due to the higher translation of the products from reaction on the Π state.

It should be noted that the blue and red wings need not necessarily arise from reaction across two separate surfaces. In the model study performed in this laboratory[3] trajectories were run on only one upper state surface. However, both blue and red wings were generated since trajectories could sample configurations where the differences between the upper and lower potentials could be either to the blue or to the red of the asymptotic potential difference. In this case the relative intensities of the red and the blue wings were determined by the dynamics (the characteristic reactive pathway, which depends on the nature of the energy release) on the single upper surface.

ACKNOWLEDGMENTS

We are indebted to a number of colleagues for helpful discussions, most especially A. Gallagher, J.L. Gole, F. Engelke, A.D. May, and H.L. Welsh. This work was made possible by support from the National Sciences and Engineering Research Council of Canada (NSERC). S.H.P.B. thanks NSERC for the award of a scholarship.

APPENDIX A: DENSITY CALCULATIONS

It is necessary to know the densities of reagents, and other gases, in the viewing zone, in order to calculate the expected intensity of D line emission (Appendix B) and the extent of secondary broadening (Appendix D). The pressures of gases in the reaction zone were calculated for a point 1.5 cm below the end of the discharge tube and 6 cm from the nozzle of the oven.

The pressures of CF_4 and He were estimated using values obtained by Skrlac in this laboratory [Skrlac (unpublished results)] measured for CO_2 in a reaction vessel nearly identical to the one described here. The

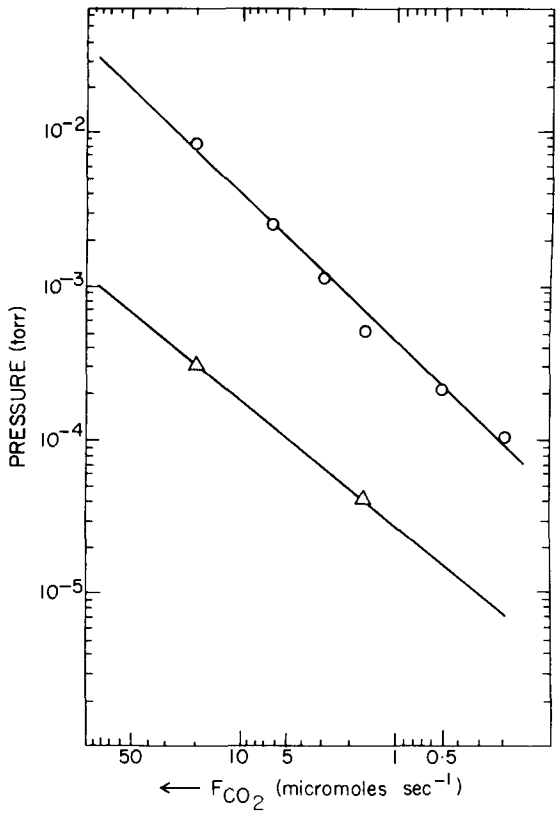

FIG. 10. Pressure of CO_2 as a function of CO_2 flow, F_{CO_2} at two positions in the reaction vessel. Points designated by o were measured at the end of the discharge tube. Points designated Δ were measured 1.5 cm below the end of the discharge tube.

data are shown in Fig. 10. Pressure measurement was made using a moveable tube, perpendicular to the line of flow.

The pressure of F atoms in the reaction zone was calculated using the pressure obtained for CF_4 and multiplying by the estimated yield of 2F atoms per CF_4 molecule. This average number of F atoms formed per CF_4 molecule dissociated was obtained from comparison with discharged F_2.

The pressures of atomic sodium and sodium dimer in the reaction zone were calculated as follows: First the equilibrium vapor pressures of Na and Na_2 were obtained for the given temperature of the oven body T_O using the equations

$$\log_{10}(p_{Na}) = 7.459 - \frac{5309}{T_O} \tag{A1}$$

and

$$\log_{10}(p_{Na_2}) = 7.596 - \frac{6307}{T_O} \tag{A2}$$

(fitted to data from the JANAF tables[29]). In Eqs. (A1) and (A2) p_{Na} and p_{Na_2} are in Torr and T_O is in K. The equilibrium constant $K_{eq}(T)$ for dissociation of Na_2 was also obtained from Eqs. (A1) and (A2). The nozzle was always hotter than the oven body and the effect this had on P_{Na} and P_{Na_2} ahead of the nozzle was taken into account by calculating the equilibrium constant for the temperature of the nozzle $K_{eq}(T_N)$ and solving for the amount of dimer x which dissociated using

$$\frac{(p_{Na} + 2x)^2}{(p_{Na_2} - x)} = 760 K_{eq}(T_N) \ . \tag{A3}$$

Thus $(p_{Na} + 2x)$ gave the pressure of atomic sodium and $(p_{Na_2} - x)$ gave the pressure of sodium dimer ahead of the nozzle. Values for [Na] and [Na_2] in the reaction zone were then calculated using

$$n = \frac{n_0}{4}\left(\frac{r}{L}\right)^2 , \tag{A4}$$

derived from the equation for effusive flow.[51] In Eq. (A4) n_0 is the density ahead of the nozzle in particles cm^{-3}, n is the density on axis at a distance L from the source and r is the radius of the nozzle. The effusive flow equation was used as the basis of the density estimates since previous work[28] has shown that supersonic expansions of Cs and Rb vapors yielded beam intensities which were approximately equal to intensities calculated for effusive beams.

To account for the fact that there was dimer formed in the expansion from the nozzle, another method of calculating the number density of Na_2 in the reaction zone was used. First, from the method given above an equilibrium dimer mole fraction F_e ahead of the nozzle was calculated. Then a value for the dimer mole fraction F_s formed in the supersonic expansion was obtained from Bergmann's results.[30] Then [Na_2] was calculated from

$$n' = n(1 + F_s/F_e) \ ,$$

where n is the number density calculated from Eq. (A4) and n' is the number density calculated when account was taken of the dimers formed in the expansion. The decrease in [Na] due to dimer formation in the beam was taken into account by subtracting from [Na] twice the increase in [Na_2].

Since our conditions differed from Bergmann's, the degree to which dimers were formed in the expansion is not well known for the experiments described here. Consequently, for the estimates of [Na] and [Na_2] used in the following Appendices the values calculated by the two methods set out above were averaged.

APPENDIX B: *D* LINE INTENSITY CALCULATION

For calculation of the *D*-line signal expected from reaction (1) of the text,

$$F + Na_2 \rightarrow NaF + Na^*(3\,^2P) \ ,$$

it was necessary to estimate the pressure of reagents in the reaction zone (Appendix A), the rate constant for the reaction k_1, the volume of emitters observed, and the detection efficiency.

For the steady state conditions of the experiments described here the rate of formation of Na* was approximately equal to the rate of removal by radiation.[52] The rate of removal by radiation was just the total number of *D* line photons radiated per second per unit volume. Therefore the observed signal in counts s^{-1}

at the D line, I_D is given by the equation

$$I_D = \int k_1[F][Na_2]\mathfrak{D}\, dV \ , \tag{B1}$$

where k_1 is the rate constant for reaction (1), [F] and [Na_2] are the concentrations of F atoms and Na_2, respectively, and $\mathfrak{D}$ is the detection efficiency. The integral is taken over volume.

The calculation set out in this Appendix was performed using only average quantities for the terms in the integral, over the volume of observation. Hence

$$I_D = k_1[F]_{av}[Na_2]_{av}\mathfrak{D}V \ .$$

The conditions used for this calculation are found in Table I of Sec. III. These conditions were chosen because the experimentally observed value for I_D fell in the middle of the range of I_D observed during the experiments on emission from $FNaNa^{\dagger}*$.

Reagent pressures were calculated as outlined in Appendix A. For a CF_4 flow of 0.4 μmol s^{-1} the pressure of F atoms was $\sim 3\times10^{-5}$ Torr. For F atoms at 300 K this corresponds to a [F] of 0.8×10^{12} atoms cm^{-3}. For the conditions of Table I of the text the [Na_2] in the reaction zone was calculated to have been $\sim 2\times10^{10}$ molecules cm^{-3} corresponding to a pressure of $\sim 4\times10^{-6}$ Torr.

The volume observed had an area of 0.1 cm^2 (spectrometer slit area) and a depth of 16 cm limited by a baffle at the front and the back of the reaction zone; hence $V = 1.6$ cm^3. Average reagent pressures across the depth of this reaction zone were calculated. The density profile (along the viewing axis) was obtained assuming a $\cos\Theta$ and $1/r^2$ dependence from the sources. This had the effect that $[F]_{av}[Na_2]_{av} = 0.19[F][Na_2]$.

The value of k_1 is not known but can be estimated, by analogy with the reaction Cl + Na_2. The cross section for this reaction is ~ 40 $Å^2$.[17,21] From the harpooning model one expects a similar cross section for F + Na_2 and Cl + Na_2. To calculate k_2, we need the effective temperature.

A temperature of 600 K was taken for the Na_2 reagent, a temperature of 300 K for the F atoms. Using the equations[53]

$$T^* = \frac{m_1T_2 + m_2T_1}{m_1 + m_2} \ ,$$

$$\bar{v} = 14\,551(T^*/\mu)^{1/2} \ ,$$

$$k_1 = \sigma\bar{v} \ ,$$

k_1 was calculated to be $\sim 3\times10^{-10}$ cm^3 $molecules^{-1}$ s^{-1}.

The value of the detection efficiency $\mathfrak{D}$ was obtained by focusing the radiation from the aperture of a blackbody onto the slit of the spectrometer and comparing the expected signal, S_{BB} with the observed signal S. The value of $\mathfrak{D}$ was $\sim 1\times10^{-6}$.

Using the estimated values for the parameters; k_1 $\sim 3\times10^{-10}$ cm^3 $molecules^{-1}$ s^{-1}, $[F]_{av}[Na_2]_{av} \sim 3\times10^{21}$ $molecules^2$ cm^{-6}, $\mathfrak{D} \sim 1\times10^{-6}$, and $V \sim 1.6$ cm^3, the value calculated for I_D was 1.5×10^6 counts s^{-1}. The measured value of I_D was 2.4×10^6 counts s^{-1}.

APPENDIX C: LORENTZ AND DOPPLER BROADENING

The normalized Lorentz line shape $g(\nu)$ of an isolated spectral line is given by

$$g(\nu) = \frac{2\tau}{1 + 4\pi^2(\nu - \nu_0)^2\tau^2} \ , \tag{C1}$$

where ν_0 is the frequency at the center of the line, ν is the frequency, and τ is the natural lifetime.[54] For $Na^*(3\,^2P)$ τ is 16.5 ns.[55] For the wavelengths of interest $g(\nu) \simeq (2\pi^2(\nu - \nu_0)^2\tau)^{-1}$. The Lorentz wings are calculated from the convolution of the line shape function with the detection system transmission function. Approximating the transmission function as a triangle with an FWHM (called W) of 8.8 Å we obtain $I_{L1}(\nu)/I_{D1} = Wg_1(\nu)$ and $I_{L2}(\nu)/I_{D2} = Wg_2(\upsilon)$, where I_{L1} and I_{L2} are the Lorentz wings due to the two D lines.

The observed D line emission intensity I_D, is measured at the peak and is equal to $1.16\,I_{D2}$. The D lines were found to be in their statistical 2:1 ratio for I_{D2} (5890 Å): I_{D1}(5896 Å). Hence

$$\frac{I_L}{I_D} = \frac{1}{1.16}\left[0.5\,\frac{I_{L1}(\nu)}{I_{D1}} + \frac{I_{L2}(\nu)}{I_{D2}}\right] \ , \tag{C2}$$

where I_L/I_D is the calculated contribution to I_W/I_D due to the Lorentz wing.

For wavelengths greater than 70 Å from the D line, the Lorentz wings are less then 7% of the blue wing, and hence are negligible. At wavelengths closer to the D line the blue wing is flattened by subtraction of the Lorentz wing. For example, at about 5860 Å, the calculated Lorentz wing is $\sim$ 50% of the measured wing. In the red wing, the Lorentz contribution is at most only 20% of the measured wing at the wavelength nearest to the D line. The rise in intensity of the red wing toward the D-line wavelength is virtually unaffected by subtraction of the calculated Lorentz wing. Rising intensity in the portion of the blue wing nearest to the D line is still consistent with the data since the correction for the Lorentz wings is uncertain due to significant uncertainty in the wavelength scale, particularly when scanning wavelengths.

Doppler broadening is certainly negligible for all regions of the experimentally determined wings.

The Doppler shifted frequency of a photon of frequency ν_0 emitted in a given direction (say the x axis) from a source with velocity component v_x is

$$\nu = \nu_0\left(1 + \frac{v_x}{c}\right) \ , \tag{C3}$$

where c is the speed of light.

For a thermal distribution of emitters the normalized Doppler line shape is[54]

$$g(\nu) = \left(\frac{c}{\nu_0}\right)\left(\frac{M}{2\pi kT}\right)^{1/2}\exp\left[-\frac{M}{2kT}\,\frac{c^2}{\nu_0^2}(\nu - \nu_0)^2\right] , \tag{C4}$$

where M is the mass of the emitter, k is Boltzmann's constant, and T is the temperature of the emitter. Since the distribution of emitters would only by chance

be a thermal distribution, Eq. (C3) was used. The exothermicity for the reaction

$$F + Na_2 \rightarrow NaF + Na^*(3\,^2P)$$

is about 58 kcal mol^{-1}. Assuming that all this energy goes into v_x of Na*$(3\,^2P)$ the value of v_x for Eq. (C3) was calculated to be $\sim 5\times10^5$ cm s^{-1}. Thus, v_x/c was $\sim 1.6\times10^{-5}$. Since $\nu_0 \sim 5\sim 10^{14}$ Hz (the D line frequency), the maximum possible shift in the frequency was calculated to be $\sim 8\times10^9$ Hz, which is about 300 times closer to line center than observed in the experiments on FNaNa‡*. Clearly, by this argument, Doppler broadening is entirely negligible in the region of the observed wings.

Alternatively, Eq. (C4) was used for an approximate calculation of the contribution of Doppler broadening to the observed wings. A temperature of 10 000 K was assumed for the Na* emitters. This temperature was a reasonable value for a translational temperature.[17,27] On this assumption, 30 Å (or 2.6×10^{12} Hz) from line center $g(\nu)/g(\nu_0) \approx \exp(-3.3\times10^5)$, an entirely negligible value.

APPENDIX D: SECONDARY BROADENING

Calculations were made to estimate the amount of secondary broadening present in the experiments on emission from FNaNa‡*. Secondary broadening refers to broadening of the Na* line due to emission during a collision with another species. The species for which detailed calculations were performed were F, Na, He, Na_2, and CF_4.

In order to obtain an estimate of the secondary broadening which could have given emission at the frequencies observed in the experiments on FNaNa‡*, the quasistatic theory of line broadening was used. For a thermal ensemble of emitters and perturbers, in the absence of trapping, the equation for the ratio of the intensity of wing emission $I'(\nu, T)$ in photons s^{-1} to the intensity of the D line $I'(\nu_0, T)$ in photons s^{-1}, is[13]

$$\frac{I'(\nu,T)}{I'(\nu_0,T)} = Wn_0\left(\frac{\nu}{\nu_0}\right)^3 4\pi R^2 \sum_i P_i(R,T)\left|\frac{d\nu_i}{dR}\right|^{-1} \qquad \text{(D1)}$$

and

$$P_i(R,T) = (g_i/g_A)\exp -[V_u(R) - V_u(\infty)]/kT\ , \qquad \text{(D2)}$$

where W is the bandwidth of the spectrometer, n_0 is the density of perturber gas, ν is the frequency of the wing emission, ν_0 is the frequency of the atomic line, R is the separation of Na* from the perturber, g_i and g_A are the degeneracies of the molecular and atomic state, respectively, $V(R)$ is the potential in which the nuclei move, and $P_i(R, T)$ is the probability of finding the perturber at distance R for temperature T.

Using Eqs. (D1) and (D2) and perturber densities calculated as outlined in Appendix A for the conditions of Table I of the text, the contribution of secondary broadening to the wings was calculated.

The secondary broadening of Na* by Na was calculated for the wavelength 5956 Å. The parameters needed for Eqs. (D1) and (D2) were obtained from potential curves for Na_2.[56,57] Using the potentials of Konowalow *et al.*[56] it was found that the only transitions which contributed to secondary broadening were $A\,^1\Sigma_u^+ \rightarrow X\,^1\Sigma_g^+$, and $^3\Sigma_g^+ \rightarrow {}^3\Sigma_u^+$. In addition, these calculated potentials suggested that the contributions from these transitions were approximately equal. From accurate potentials for the X and A states of Na_2 given by Zemke *et al.*[57] it was calculated that a potential energy separation corresponding to emission at 190 cm^{-1} to the red of the D line (i.e., at 5956 Å) occurred for a value of R of 12 Å and, at this value of R, $|d\nu/dR|$, required for Eq. (D1), was found to be 38 cm^{-1} Å^{-1}. The value of g_i/g_A in Eq. (D2) was $\frac{1}{6}$, and n_0 was 1×10^{12} from Appendix A.

For $T = 600$ K and the small difference between ν and ν_0 in this calculation the exponential term in Eq. (D2) is nearly unity. The $(\nu/\nu_0)^3$ term was also close to unity. The value of W was taken as 26 cm^{-1} for a 1 mm slit width.

Using the values of the parameters given above in Eq. (D1), the contribution to secondary broadening due to the $A \rightarrow X$ transition was calculated. This result was multiplied by a factor of 2 to account for the $^3\Sigma_g^+ \rightarrow {}^3\Sigma_u^+$ transition. This yielded a value for $I'(\nu, T)/I'(\nu_0, T)$ of 4.5×10^{-10}, showing that secondary broadening for Na* + Na collisions was negligible.

Secondary broadening by He was calculated from published experimental results.[12(d)] It was scaled to a perturber density of 4×10^{12} cm^{-3} and a bandwidth of 26 cm^{-1}. At 6000 Å and a CF_4 density of 4×10^{11} cm^{-3} $I'(\nu, T)/I'(\nu_0, T)$ was found to be 4×10^{-12}. In each case the secondary broadening is entirely negligible.

Neither accurate potentials, nor pressure broadening data could be found for either the Na*F or the Na*Na_2 system. However, the broadening due to Na is so long range (recall that the separation R was 12 Å for the frequency shift from the D line of 190 cm^{-1}) that it is reasonable to assume that this calculation sets an upper bound to the secondary broadening from any collision partner. Since $[Na_2] \leq 0.1\times[Na]$ in our experiments, the contribution of Na_2 to secondary broadening was taken as 0.1 times that calculated for Na, i.e., 4.5×10^{-11}. Since $[F] \simeq 0.8\times[Na]$, then $I'(\nu, T)/I'(\nu_0, T)$ for F was taken to be 4×10^{-10}.

Thus, the value of I_W/I_D due solely to secondary broadening totalled $\sim 9\times10^{-10}$, about three orders of magnitude less than the value of I_W/I_D observed experimentally.

APPENDIX E: TRAPPING AND SELF-ABSORPTION

In this Appendix, calculations of radiation trapping and self-absorption are described. Radiation trapping refers to the *increase in the effective radiative lifetime* of a population of emitters due to the imprisonment of resonance radiation by absorbers within the emission source.[58,59] Self-absorption refers to a *diminution in the intensity of emission* observed from a source of resonance radiation due to absorption of the radiation by the absorbers within the source. If the emission source has no absorbers the emission intensity is I_0. With absorbers present in the source the emission intensity

is I, where $I \leq I_0$.[60,61] Clearly trapping and self-absorption as defined here are simply two observable manifestations of the same physical phenomenon; the absorption of resonance radiation by absorbers within an emission source. In the experiments described here, the emitters were formed chemically by the reaction

$$F + Na_2 \rightarrow NaF + Na^*(3\,^2P) \quad (1)$$

and the absorbers were ground state sodium atoms which flowed from the oven.

The trapping calculation was based on a simple model of uniform emitter and absorber concentrations throughout a sphere with a mean escape radius ρ. The sphere was centered at the crossing point of the optical axis with the axes of flow of the reagents. It was assumed that there were no absorbers or emitters outside the sphere. In addition, the emission was assumed to be isotropic.

For a sphere with a uniform distribution of emitters and absorbers and a mean escape radius ρ the effective radiative rate β was calculated from (Holstein, 1947)

$$\beta = \gamma T(\rho) \ , \quad (E1)$$

where γ is the natural radiative rate. The so-called transmission factor $T(\rho)$ is given by[58]

$$T(\rho) = \int_{-\infty}^{\infty} P(\nu) \exp[-k(\nu)\rho]\, d\nu \ , \quad (E2)$$

where $P(\nu)$ is the normalized frequency distribution of emitters.

A full Voigt profile, the convolution of a Lorentz and Doppler profile[60,62] was used for $k(\nu)$. The Voigt profile was given by

$$k(\nu) = k_0 \frac{a}{\pi} \int_{-\infty}^{+\infty} \frac{\exp(-y^2)}{a^2 + (x-y)^2}\, dy$$

and

$$k_0 = \frac{\lambda_0^3 N \gamma}{8\pi^{3/2} v_0} \left(\frac{g_2}{g_1}\right) \ , \quad a = \frac{\gamma \lambda_0}{4\pi v_0} \ ,$$

$$x = \frac{\nu - \nu_0}{\nu_0} \ \frac{c}{v_0} \ , \quad v_0 = \left(\frac{2RT}{M}\right)^{1/2} \ ,$$

where λ_0 is the peak wavelength, N is the density of absorbers, g_2/g_1 is the ratio of the degeneracy of the upper state to that of the lower state, c is the speed of light, ν is the frequency, ν_0 is the peak frequency, R is the gas constant, T is the temperature in K, and M is the gram-molecular weight. An efficient method developed by Humlicek, was used to compute the Voigt profile.

As pointed out by Holstein[58,59] the normalized frequency distribution of emitters $P(\nu)$ is part of the full solution to the integro-differential equation which describes trapping. (This equation was derived by Holstein in the above references.) The Na* in the experiments on $FNaNa^{\dagger *}$ was formed chemically and was therefore expected to be translationally hot.[37] Thus, there were two possible limiting cases for $P(\nu)$. In one case the trapping is negligible. Therefore the steady state concentration of emitters is made up of the hot emitters formed chemically and the emission profile is determined by the translational distribution of the chemically formed Na*. In the other extreme case, the trapping is so large that the steady state concentration of emitters is, to all intents and purposes, in thermal equilibrium with the absorbers. It follows that $P(\nu) \propto k(\nu)$.

Rather than attempt to calculate the correct form for $P(\nu)$, values of $T(\rho)$ were calculated for the extreme cases discussed above for various values of [Na] and ρ. When $P(\nu) \propto k(\nu)$, calculation yielded a lower bound for $T(\rho)$. When $P(\nu)$ corresponded to the translational distribution of the Na* formed in the chemical reaction, calculation yielded an upper bound for $T(\rho)$, assuming an isotropic velocity distribution for the emitters and absorbers.

The translationally hot distributions corresponded either to a temperature or to a δ function in E_{trans}. The absorber temperature used was 600 K to allow for partial thermalization of the Na beam by the 500 K heated aperture between the oven and the reaction zone. The average emitter translational energy was between 10–20 kcal mol^{-1}. The density of Na was $\sim 10^{12}$ atoms cm^{-3}. The path length was between 2–8 cm, which corresponded to reasonable limits given the geometry of the reaction vessel. For the hot emitters the values of $T(\rho)$ fell between 0.25 and 0.6. For the (unrealistic) extreme case of cold emitters—(absorber temperature equals emitter temperature)—$T(\rho)$ fell between 5×10^{-3} and 2×10^{-2}. These estimates of trapping correspond to increases in the effective lifetime too small to give rise to a significant amount of secondary broadening, calculated as in Appendix D.

For the discussion of self-absorption the quantity of interest is I/I_0, where I_0 is the intensity which would be observed from the emission source in the absence of self-absorption and I is the emission intensity observed with self-absorption present. Several models were used to crudely represent the experimental situation.

The first model assumed an intensity I_0 incident on a layer of absorbing gas with a uniform density and of length L. The intensity I is transmitted. The ratio I/I_0 is given by

$$\frac{I}{I_0} = \frac{\int_{-\infty}^{+\infty} I(\nu) \exp[-k(\nu)L]\, d\nu}{\int_{-\infty}^{+\infty} I(\nu)\, d\nu} \ , \quad (E3)$$

where $I(\nu)d\nu$ is the intensity in $d\nu$ at frequency ν and $k(\nu)$ is the absorption coefficient.

The second model took the mixture of emitters and absorbers into account. It assumed a source which contained a uniform mixture of emitters and absorbers. Thus

$$\frac{I}{I_0} = \frac{\int_0^L \int_{-\infty}^{+\infty} I(\nu) \exp[-k(\nu)l]\, d\nu\, dl}{\int_0^L \int_{-\infty}^{+\infty} I(\nu)\, d\nu\, dl}$$

and upon integration over the length l,

$$\frac{I}{I_0} = \frac{\int_{-\infty}^{+\infty} \frac{I(\nu)}{k(\nu)} [1 - \exp(-k(\nu)L)]\, d\nu}{L \int_{-\infty}^{+\infty} I(\nu)\, d\nu} \ . \quad (E4)$$

Both of the above models gave lower bounds to I/I_0. This is because the above models are strictly one-dimensional. It was shown in this Appendix that an extreme lower bound for β was 10^6 s^{-1}. At quencher densities of 10^{12} cm^{-3}, quenching was negligible. Hence absorption of a photon led to a diminution in intensity only because of the solid angle effect, i.e., a photon which is in the cone of sight is absorbed and is re-radiated into 4π steradians. The solid angle effect is diminished by the three-dimensional nature of the source.

The third model took this diminution of the solid angle effect into account. This model assumed a spherical source with a uniform distribution of emitters and absorbers. If quenching is negligible, then, by symmetry, observation along any axis through the center of the spherical source must yield the same observed emission intensity. However, this implies that the intensity cannot be diminished by a solid angle effect. Thus, it is found that $I/I_0 = 1$.

Using hot translational temperature distributions both the first and second models gave results between 0.25 and 0.6, with only minor differences between the two models.

Since $k(\nu) \propto Ng_2/g_1$, the value of I/I_0 differs for the two D lines. Therefore the ratio of the D lines acted as a measure of the extent of self-absorption. The ratio of the resolved D lines was measured at flows of Na greater than or equal to those used in the experiments on $FNaNa^{\dagger *}$. The ratios of the D lines were measured at 1.82 ± 0.02 and 1.98 ± 0.02 (reading error and photon statistics only included in the above error estimates), respectively. These values of $I_D(^2P_{3/2})/I_D(^2P_{1/2})$ indicated that I/I_0 was between 0.5–1.0.

A major weakness in the models used for the above calculations is the fact that they ignore the directionality of the Na beam, i.e., an isotropic velocity distribution of the Na had been assumed. The directionality was clearly evident in the experiments, since the Na deposit formed "shadows" on the far side of the reaction vessel. The assumption of an isotropic velocity distribution for the Na absorbers exaggerated the amount of self-absorption. Emission from the Na* formed in the $F + Na_2$ reaction had substantial Doppler breadth along the spectrometer's optical axis. The absorbing gas was moving preferentially along a line perpendicular to the optical axis. Hence the absorbers exhibited only a very narrow absorption coefficient $k(\nu)$. Therefore it is likely that I/I_0 was ~1 for the F + Na system.

It should be noted that the argument concerning the directionality of the Na beam also applies to the trapping phenomenon since trapping is due to nothing more than multiple absorptions and re-emissions. This suggests that β (the effective radiative rate) was probably approximately equal to γ (the natural radiative rate), i.e., trapping was also negligible.

[1]For a review see T. Carrington Jr., J. C. Polanyi, and R. J. Wolf, in *Physics Electronic and Atomic Collisions*, edited by S. Datz (North Holland, Amsterdam, 1982), p. 393.
[2]H.-J. Foth, H. R. Mayne, R. Poirier, and J. C. Polanyi, *Lasers and Photochemistry and Photobiology*, edited by Ahmed H. Zewail (Harwood Academic, New York, 1983).
[3]J. C. Polanyi and R. J. Wolf, J. Chem. Phys. **75**, 5951 (1981).
[4](a) For references to extensive work by T. F. George and co-workers see: T. F. George, J. Phys. Chem. **86**, 10 (1982); (b) A. M. F. Lau, Phys. Rev. A **13**, 139 (1976); **14**, 279 (1976); Phys. Rev. Lett. **43**, 1009 (1978); Phys. Rev. A **22**, 614 (1980); (c) V. S. Dubov, L. I. Gudzenko, L. V. Gurvich, and S. J. Yakovlenko, Chem. Phys. Lett. **45**, 330 (1977); S. I. Yakovlenko, Sov. J. Quantum Electon. **8**, 151 (1978); (d) A. E. Orel and W. H. Miller, Chem. Phys. Lett. **57**, 362 (1979); J. Chem. Phys. **70**, 4393 (1979); (e) J. C. Light and A. Altenberger-Siczek, *ibid.* **70**, 4108 (1979).
[5]For a recent review see R. S. Berry, in *Physics Electronic and Atomic Collisions*, edited by S. Datz (North Holland, Amsterdam, 1982), p. 413.
[6]P. Hering, P. R. Brooks, R. F. Curl, Jr., R. S. Judson, and R. S. Lowe, Phys. Rev. Lett. **44**, 687 (1980).
[7]P. R. Brooks, R. F. Curl, and T. C. Maguire, Ber. Bunsenges. Phys. Chem. **86**, 401 (1982).
[8]H. P. Grieneisen, Hu Xue-Jing, and K. L. Kompa, Chem. Phys. Lett. **82**, 421 (1981).
[9]B. E. Wilcomb and R. E. Burnham, J. Chem. Phys. **74**, 6784 (1981).
[10]P. Arrowsmith, P. E. Bartoszek, S. H. P. Bly, T. Carrington, Jr., P. E. Charters, and J. C. Polanyi, J. Chem. Phys. **73**, 5895 (1980), paper I of this series.
[11]J. C. Polanyi, Faraday Discuss. Chem. Soc. **67**, 129 (1979).
[12](a) D. L. Drummond and A. Gallagher, J. Chem. Phys. **60**, 3426 (1974); (b) G. York, R. Scheps, and A. Gallagher, *ibid.* **63**, 1052 (1975); (c) W. P. West, P. Shuker, and A. Gallagher, *ibid.* **68**, 3864 (1978), and references therein; (d) M. D. Havey, S. E. Frolking, and J. J. Wright, Phys. Rev. Lett. **45**, 1783 (1980).
[13]R. E. M. Hedges, D. L. Drummond, and A. Gallagher, Phys. Rev. A **6**, 1519 (1972).
[14]M. G. Evans and M. Polanyi, Trans. Faraday Soc. **35**, 178 (1939).
[15]J. L. Magee, J. Chem. Phys. **8**, 687 (1940).
[16]W. S. Struve, T. Kitagawa, and D. R. Herschbach, J. Chem. Phys. **54**, 2759 (1971).
[17]W. S. Struve, J. R. Krenos, D. L. McFadden, and D. R. Herschbach, J. Chem. Phys. **62**, 404 (1975).
[18]P. K. Pearson, W. J. Hunt, C. F. Bender, and H. F. Schaefer III. J. Chem. Phys. **58**, 5358 (1973).
[19]G. G. Balint-Kurti, Ph.D. thesis, Harvard University, 1969.
[20]G. G. Balint-Kurti and M. Karplus, in *Orbital Theories of Molecules and Solids*, edited by N. H. March (Oxford University, Clarendon, 1974), p. 250.
[21]W. S. Struve, Mol. Phys. **25**, 777 (1973).
[22]F. E. Bartoszek, B. A. Blackwell, J. C. Polanyi, and J. J. Sloan, J. Chem. Phys. **74**, 3400 (1981).
[23]K. B. Woodall, Ph.D. thesis, University of Toronto, 1971.
[24]B. Kasemo and L. Wallden, Surf. Sci. **53**, 393 (1975).
[25]J. W. Hepburn, Ph.D. thesis, University of Toronto, 1980.
[26]F. E. Bartoszek, Ph.D. thesis, University of Toronto, 1980.
[27]S. H. P. Bly, Ph.D. thesis, University of Toronto, 1982.
[28]R. J. Gordon, Y. T. Lee, and D. R. Herschbach, J. Chem. Phys. **54**, 2393 (1971).
[29]*JANAF Thermochemical Tables* (Dow Chemical, Midland, 1965).
[30]K. Bergmann, U. Hefter, and P. Hering, Chem. Phys. **32**, 329 (1978).
[31]A. Hermann, S. Leutwyler, E. Schumacher, and L. Woste, Helv. Chim. Acta. **61**, 453 (1978).
[32]M. Hofmann, S. Leutwyler, and W. Schulze, Chem. Phys. **40**, 145 (1979).
[33]D. O. Ham, J. Chem. Phys. **60**, 1802 (1974).
[34]R. C. Oldenborg, J. L. Gole, and R. N. Zare, J. Chem. Phys. **60**, 4032 (1974).

[35]C. E. Kolb and M. Kaufman, J. Phys. Chem. **76**, 947 (1972).
[36]P. R. Bevington, *Data Reduction and Error Analysis for the Physical Sciences* (McGraw–Hill, New York, 1969).
[37]P. Arrowsmith, S. H. P. Bly, P. E. Charters, J. C. Polanyi, and H. H. Telle, Chem. Phys. (in press).
[38]L. K. Lam, A. Gallagher, and M. M. Hessel, J. Chem. Phys. **66**, 3550 (1977).
[39]L. K. Lam, T. Fujimoto, A. C. Gallagher, and M. M. Hessel, J. Chem. Phys. **68**, 3553 (1978).
[40]W. H. Crumley, J. L. Gole, and D. A. Dixon, J. Chem. Phys. **76**, 6439 (1982).
[41]K. P. Huber and G. Herzberg, *Constants of Diatomic Molecules* (Van Nostrand Reinhold, New York, 1979).
[42]R. L. Martin and E. R. Davidson, Mol. Phys. **35**, 1713 (1978).
[43]J. L. Gole, G. J. Green, S. A. Pace, and D. R. Preuss, J. Chem. Phys. **76**, 2247 (1982).
[44]R. S. Berry, in *Alkali Halide Vapours*, edited by P. Davidovitz and D. L. McFadden (Academic, New York, 1979), p. 78.
[45]D. O. Ham and H. W. Chang, Chem. Phys. Lett. **24**, 579 (1974).
[46]E. Kay, J. Coburn, and A. Dilks, in *Topics in Current Chemistry ; Plasma Chemistry III*, edited by S. Veprek and M. Venugopalan (Springer, Berlin, 1980), p. 1.
[47]R. N. Sileo and T. A. Cool, J. Chem. Phys. **65**, 117 (1976).
[48]F. Engelke, Chem. Phys. Lett. **65**, 564 (1979).
[49]P. J. Kuntz, M. H. Mok, and J. C. Polanyi, J. Chem. Phys. **50**, 4623 (1969).
[50]J. C. Polanyi and J. L. Schreiber, Faraday Discuss. Chem. Soc. **62**, 267 (1977).
[51]S. Dushman, *Scientific Foundations of Vacuum Techniques*, edited by J. M. Lafferty (Wiley, New York, 1962).
[52]J. R. Krenos, K. H. Bowen, and D. R. Herschbach, J. Chem. Phys. **63**, 1696 (1975).
[53]J. Ross, J. C. Light, and K. E. Shuler, in *Kinetic Processes in Gases and Plasmas*, edited by A. R. Hochstim (Academic, New York, 1969), p. 281.
[54]A. Yariv, *Quantum Electronics* (Wiley, New York, 1975).
[55]A. Lindgard and S. E. Nielsen, At. Data Nucl. Data Tables **19**, 534 (1977).
[56]D. D. Konowalow, M. E. Rosenkrantz, and M. L. Olson, J. Chem. Phys. **72**, 2612 (1980).
[57]W. T. Zemke, K. K. Verma, T. Vu, and W. C. Stwalley, J. Mol. Spectrosc. **85**, 150 (1981).
[58]T. Holstein, Phys. Rev. **72**, 1212 (1947).
[59]T. Holstein, Phys. Rev. **83**, 1159 (1951).
[60]A. C. G. Mitchell and H. W. Zemansky, *Resonance Radiation and Excited Atoms*, (Cambridge University, Cambridge, 1934).
[61]R. D. Cowan and G. H. Dicke, Rev. Mod. Phys. **20**, 418 (1948).
[62]J. Humlicek, J. Quant. Spectrosc. Radiat. Transfer **21**, 309 (1979).